MSUCP-30
June 1980

MAGNETIC FIELD MAPPING OF THE K-500 CYCLOTRON at M.S.U.

G. Bellomo, D.A. Johnson, P. Miller, F.G. Resmini

Cyclotron Laboratory
Michigan State University, East Lansing, Michigan

Abstract

The results of an extensive magnetic field mapping of the K-500 cyclotron under construction at M.S.U., covering the entire operating range of the machine, are reported. The data are analyzed in detail, and a comparison with the theoretical calculations used in designing the cyclotron is carried out. This comparison allows one to draw some general conclusions on the reliability of the theoretical model and its implications for superconducting cyclotron design.

1. Introduction

The purpose of this paper is to report the results of an extensive magnetic field mapping of the three sector K–500 cyclotron under construction at MSU.[1] The measurements were intended to:

- provide a detailed picture of the variations of the iron-produced field, both for the azimuthal modulation and the average field, over the entire operating range of the cyclotron.
- allow a comparison with previous calculations, so as to establish the reliability of the latter.
- check the existence of imperfections.
- determine if modifications of the pole tip geometry were needed in order to achieve the appropriate field for the cyclotron.

This paper deals with the first three topics, since field corrections and its trimming are extensively reported elsewhere[2]. All maps were taken using the field measuring apparatus described in (3). For the present purposes we may just recall that 54 flip-coils are spaced at .5" intervals from 0" to 26.5" radius, along a radially positioned bar, so that all data corresponding to a given azimuth are taken at once, by flipping the coils twice through 180°. Azimuthal intervals were 2° for all maps. The entire data-taking process (flipping-storage-azimuthal movement) is computer controlled and typically a 360° map in 2° intervals takes about four and a half hours. The overall precision of the measurements,

taking into account calibration errors, temperature corrections, etc. is about $\pm$ .03%. While this was judged entirely adequate for the present purposes, several improvements are planned for later mappings with the final field configuration in order to bring the error down to $\pm$ 0.01%.

2. Pole geometry

We shall briefly review the pole geometry relevant to these field maps. It differs from the one used in earlier field measurements[3] only by the presence of the center plug, which has been designed to allow the insertion of the internal source.

2.1 Pole tip geometry

A perspective view of a hill and a valley is given in Fig. 1, while the radial profiles relative to the median plane are given in Fig. 2. The pole radius is 25.75", but the iron structure, as shown clearly in Fig. 1, continues as part of the inner tank wall from 26" to 28" radius both for the hill and the valley. There is therefore a 1/4" radial gap between the two iron structures. A central hole of 3.5" radius is provided for the plug insertion.

The upper part of the hill, 5.75" thick, is flat, providing a 2.5" constant axial gap between 3.5" and 25.75" radius, and has an average spiral constant of 1/13 (rad/inch). The hill is actually machined into two pieces in order to approximate the said spiral with two arcs of circles. The first

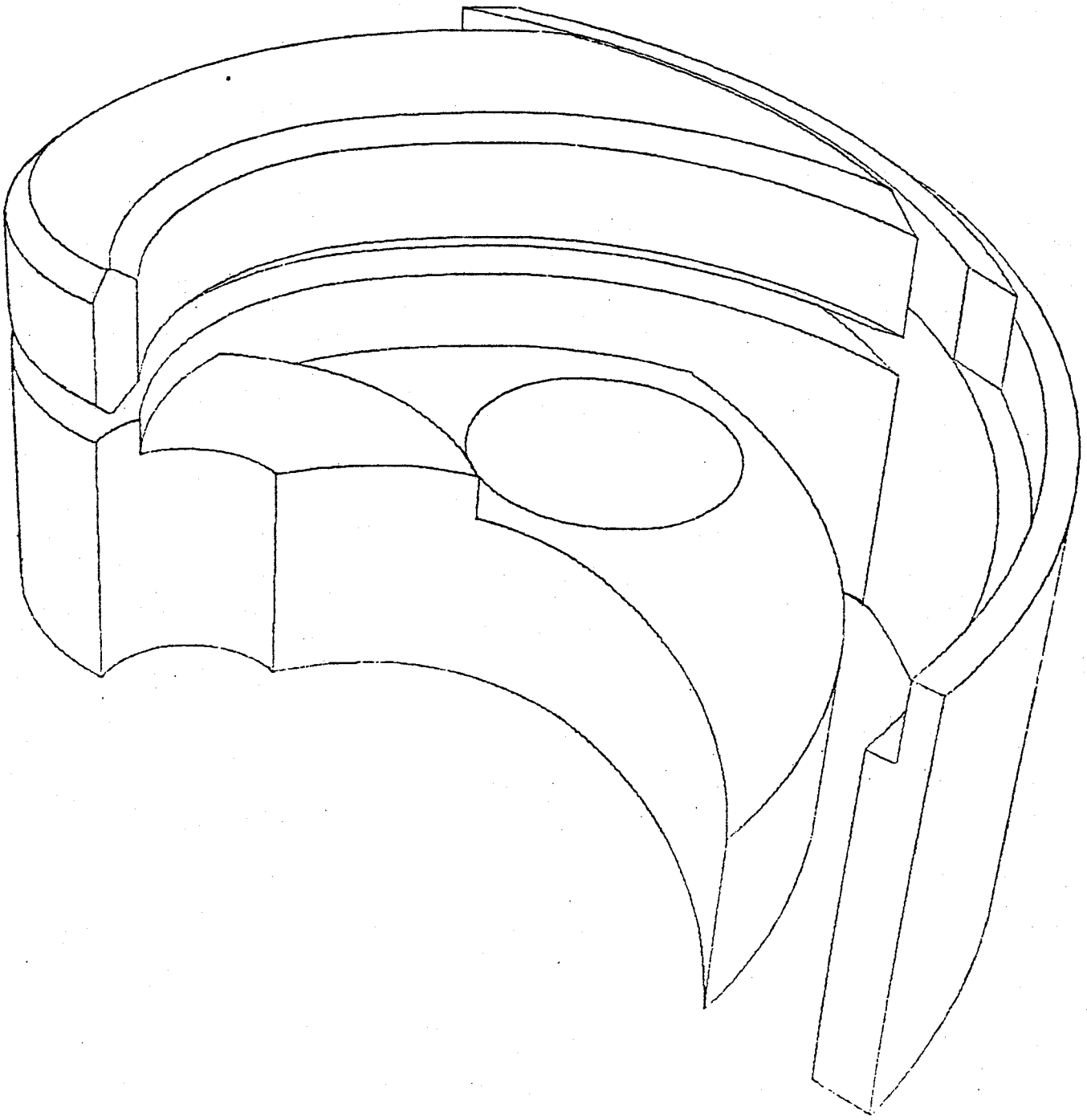

FIG. 1. Perspective view of a sector for the K-500 pole tip geometry.

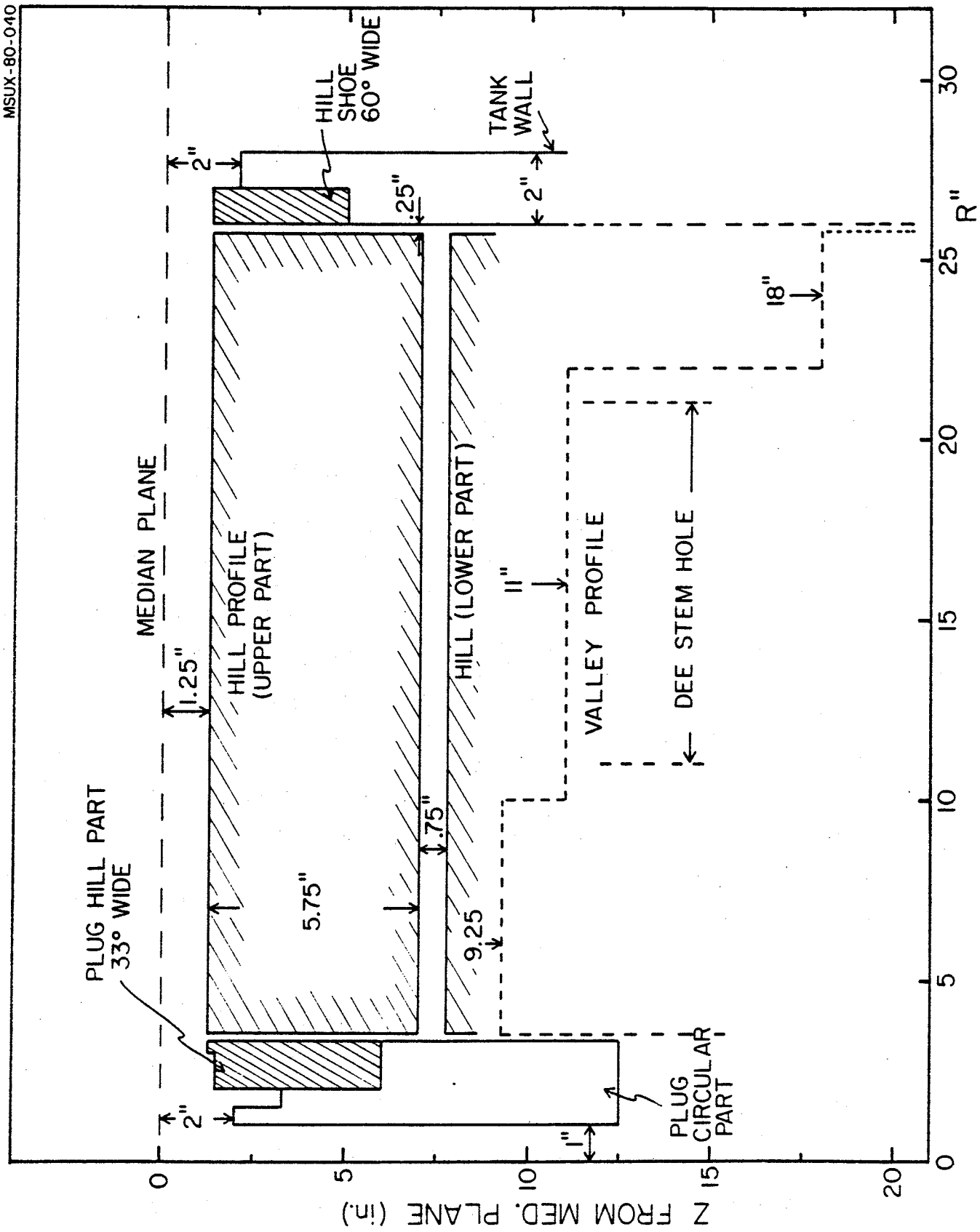

FIG. 2. Radial hill and valley profile of the pole tip geometry.

section runs up to a radius of 13.93", the second up to 25.75". The effects of this splitting on the field will be seen in the following.

The hill is chamfered on both azimuthal edges at 45^{o}, as apparent from Fig. 1, the width of the tapering being .85" axially and azimuthally. The azimuthal width of the hill itself, including the chamfered section, starts from 33^{o} at 3.5" radius, and reaches 46^{o} at about 10" radius, being then essentially constant up to 25.75". The hill shoe inserted in the inner tank wall between 26" and 27" provides also a 2.5" axial gap, but it is 60^{o} wide, centered along the continuation of the spiral, to compensate for the 1/4" radial gap mentioned above. The ring between 27" and 28" in radius provides a 4" axial gap for both hill and valleys.

The valley shimming is well apparent from both Figs. 1 and 2. The resulting axial gap is 18.5" from a radius of 3.5" to 10", 22" from 10" to 22", 36" from 22" to 25.75", 10" from 26" to 27" and 4", as mentioned above, from 27" to 28". A 10" diameter hole, for the insertion of the dee stems, is provided in each valley at a radius of 16".

2.2 Central plug

The purpose of the central plug is two-fold:

- allow the insertion of the ion source through a 2" diameter center hole.
- compensate the consequent magnetic field decrease, and actually introduce a bump (or "cone") of a few hundred gauss above isochronism to properly control the phase and the axial focusing in the first few turns.

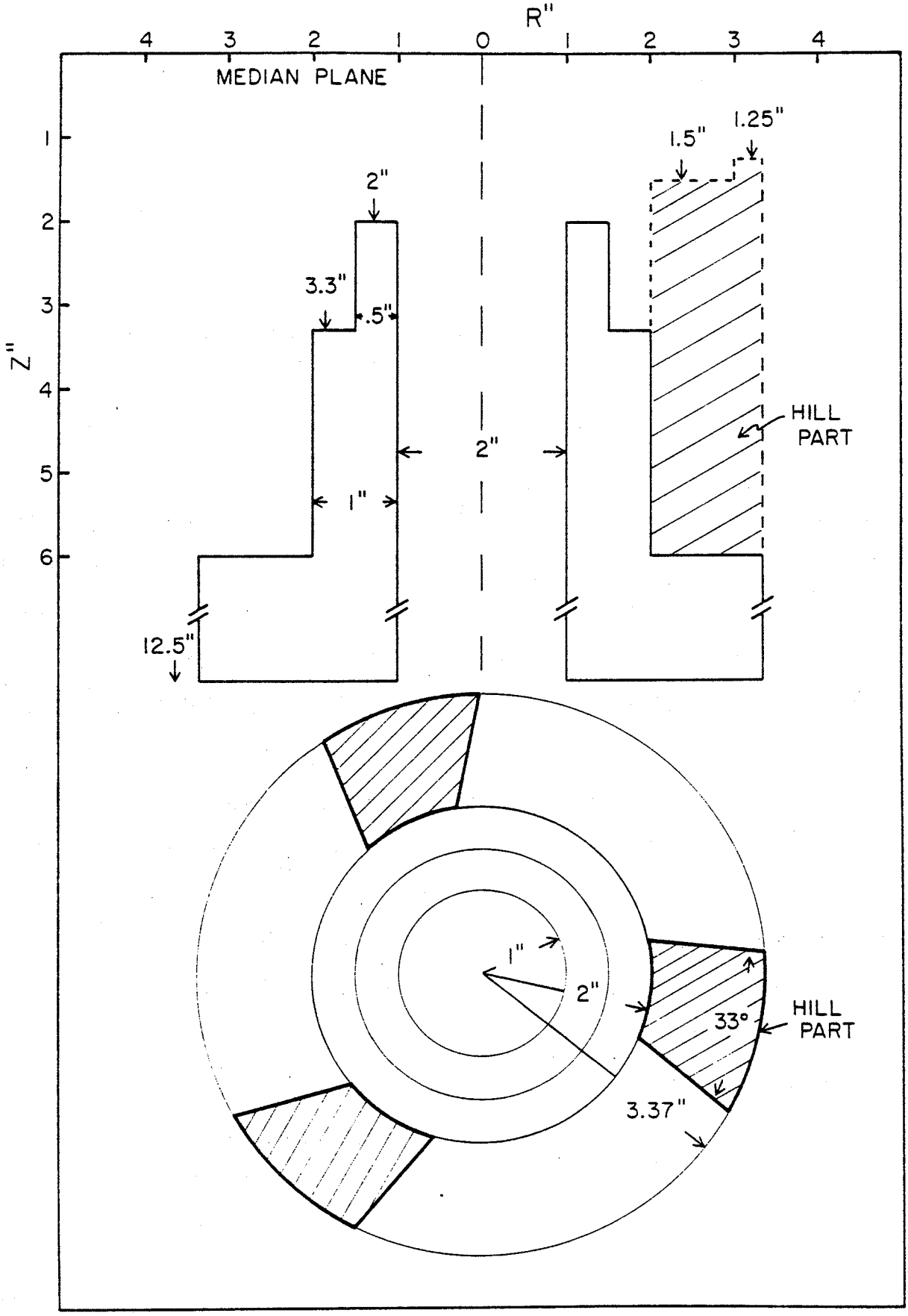

FIG. 3. Schematic vertical and median plane cross-section of the center plug.

A sketch of the plug is shown in Fig. 3. The plug is composed of a cylindrical part plus a hill part, the latter being essentially the continuation of the hills. The cylindrical part extends down to 12.5" from the median plane, has an internal diameter of 2" and an outer diameter of 6.75", to allow its insertion in the 7" magnet hole. As apparent from Fig. 3, its radial profile provides three regions of different axial gap, i.e. 4" between 1" radius and 1.5", 6.6" from 1.5" to 2", and 12" from 2" to the outer radius of 3.37". The hill part of the plug fits in the latter area, providing hill gaps of 3" from 2" to 3" in radius and of 2.50" from 3" to 3.32" radius (and therefore equal to the rest of the hill). Azimuthally this hill part is limited by two straight lines chosen as the closest approximation to the hill spiral edges starting from the center. The azimuthal width is therefore 33^{o}, like the hill at 3.5" radius, as shown also in Fig. 3.

In order to design the plug, we used the uniform saturation approximation[4] with magnetization M=21.4 kgauss. The field contributions as calculated with this method are shown in Fig. 4 both for the hill part and three different lengths of the circular part. It is seen that the length of the plug has a significant influence upon the radial extent of its field contribution. The longer the plug the more extended tends to be the effect. Therefore we chose a plug whose max. distance from the median plane, Fig. 3, is 12.5". The hill part produces instead field effects which are well confined radially.

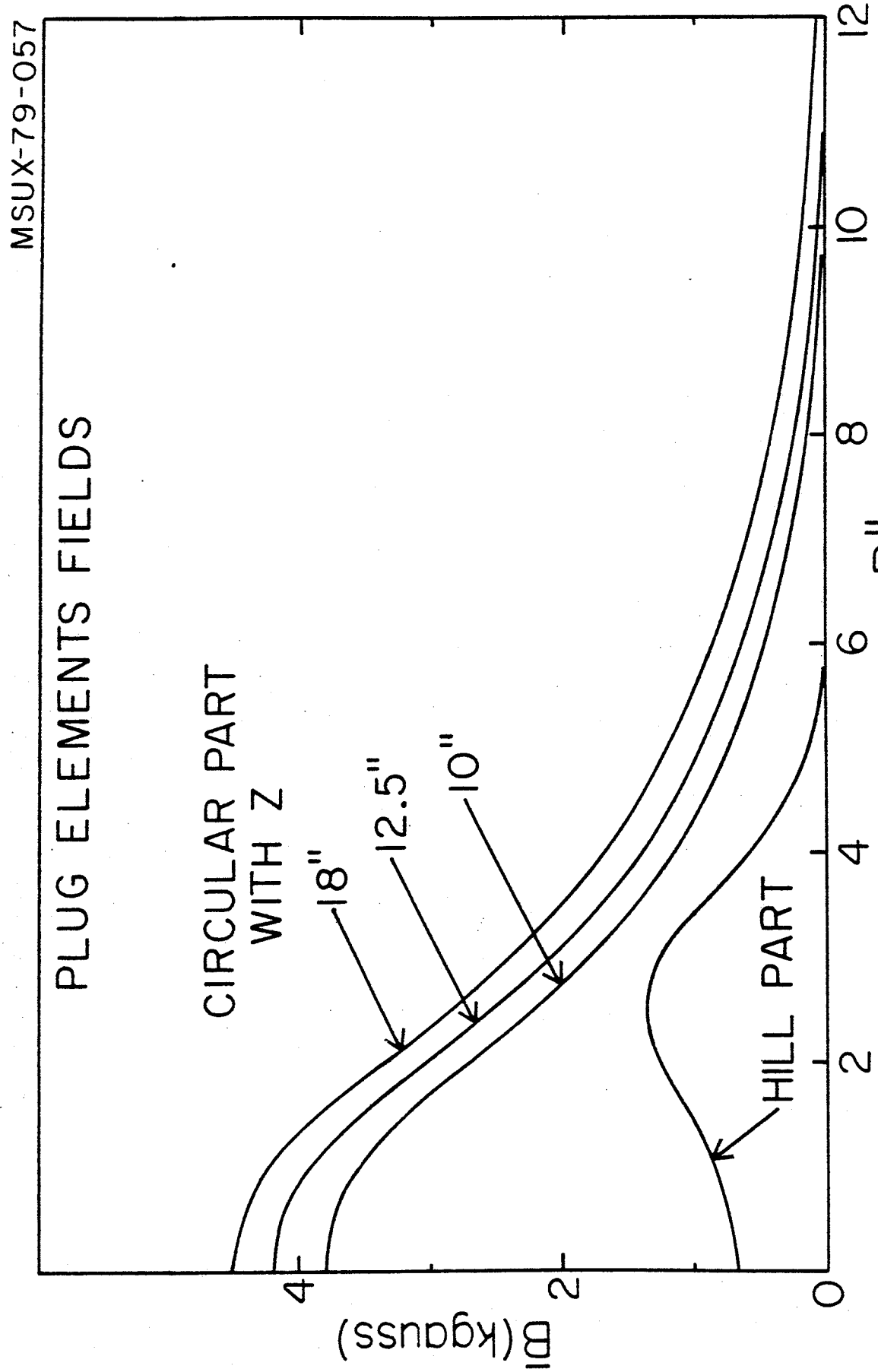

FIG. 4. Calculated field contributions for the plug hill part and three different length of the circular part. Z represents the distance of the lower surface of the plug from the median plane.

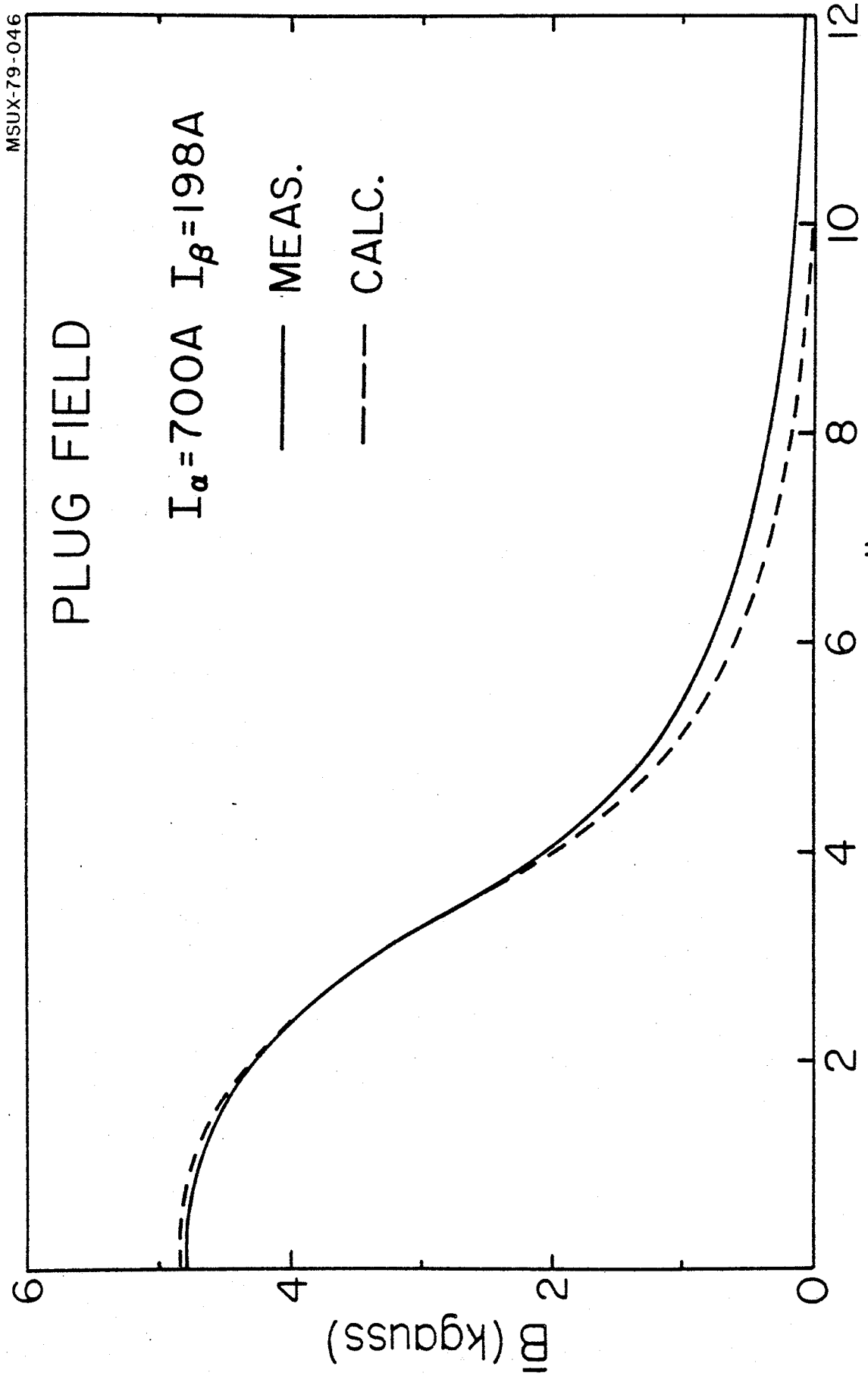

FIG. 5. Calculated and measured field contributions produced by the central plug.

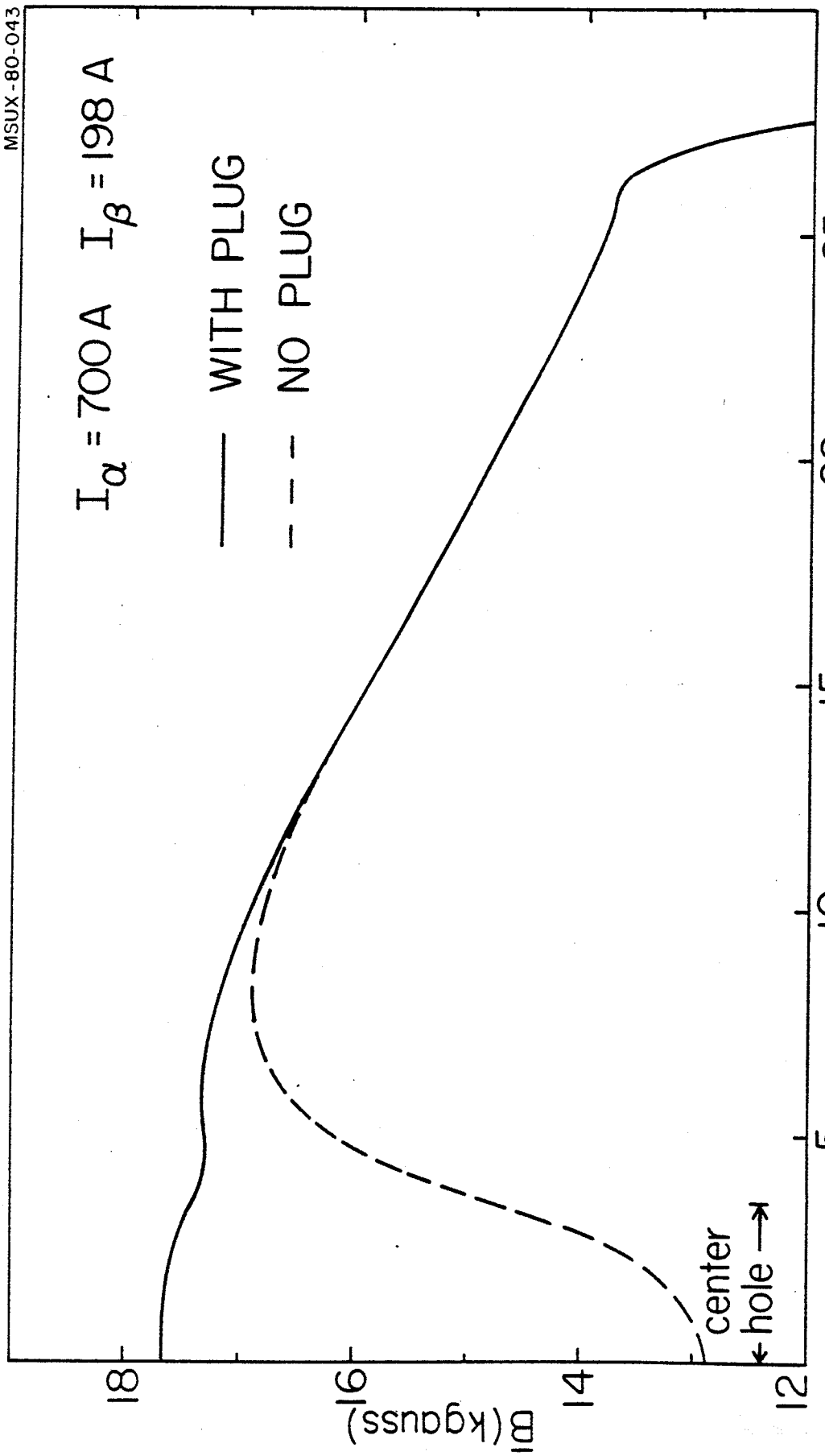

FIG. 6. Average iron produced field measured at I_α =700 A, I_β = 198 A with and without plug.

The comparison between the measured and calculated plug effects on the average field is shown in Fig. 5, the former being obviously obtained as difference from measurements with and without plug at the same excitation. The agreement looks excellent, apart from a 100-150 gauss discrepancy on the tail of the field contribution. Given the size of the maximum field correction, about 5 kgauss, this result can be considered very good. In particular, for local corrections of only a few hundred gauss one can safely predict that the uniform saturation approximation will be accurate to a few gauss.

The effect of the plug on the total iron-produced field can be seen in Fig. 6 where the measured field in absence of the plug, i.e. with the 7" diameter center hole, is also plotted.

3. Mapping range in terms of coils currents.

Let us recall that the main coils of the K-500 cyclotron are split into two parts, independently excited[1]. As shown in Fig. 7, the section closer to the median plane is about 1/3 of the total coil height. Henceforth the two sections will be referred to as small coil and large coil respectively, and their currents indicated as I_α and I_β. Also shown in Fig. 7 are the air-core fields of each section at an excitation of 700 A. The difference in shape between the two allows to approximate the required isochronous field for all particles and field levels.

In the (I_α, I_β) plane the operating diagram of the K-500 cyclotron is shown in Fig. 8. This diagram is obtained

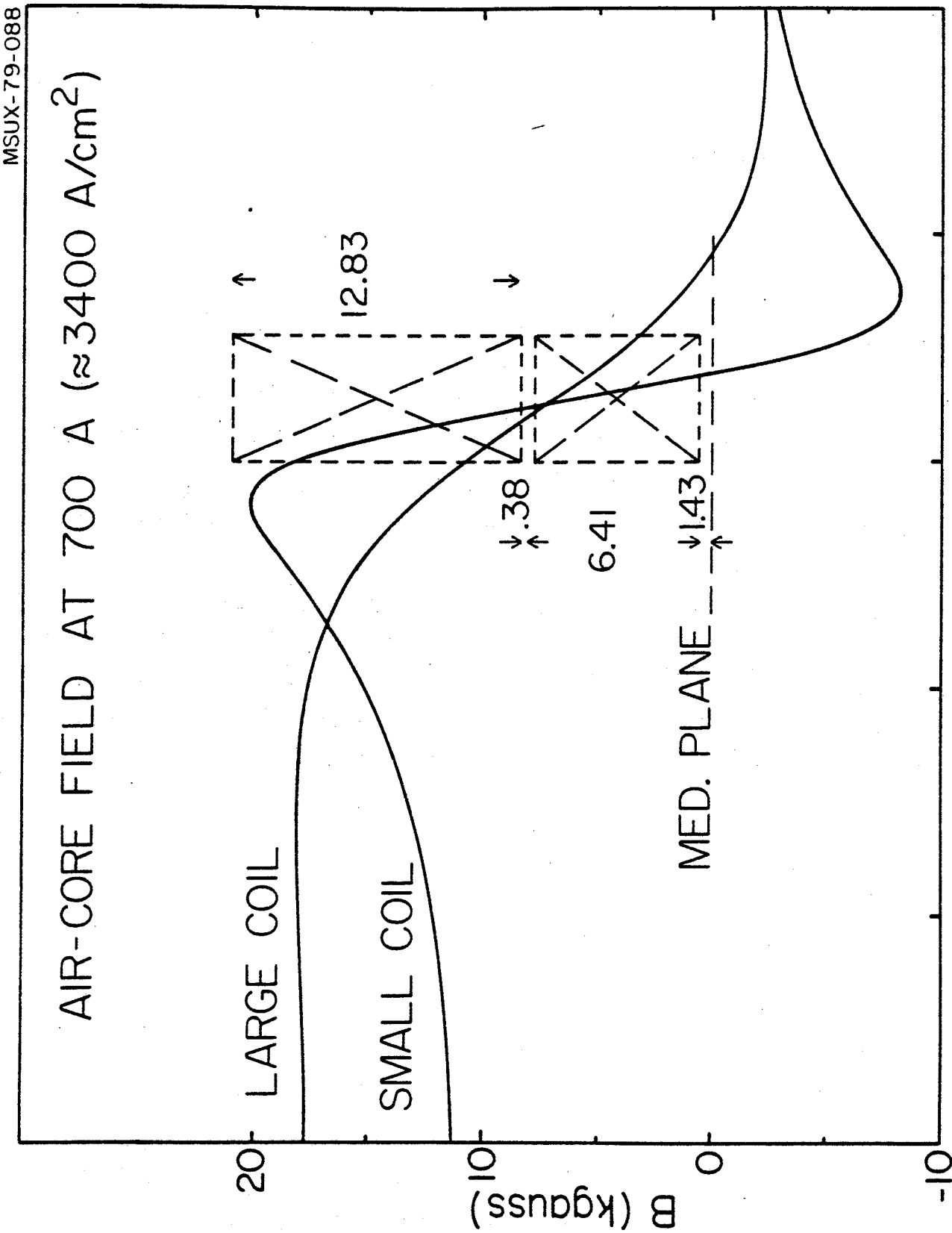

FIG. 7. Air core fields for the two main coil sections at 700 A. Coil dimensions in inches.

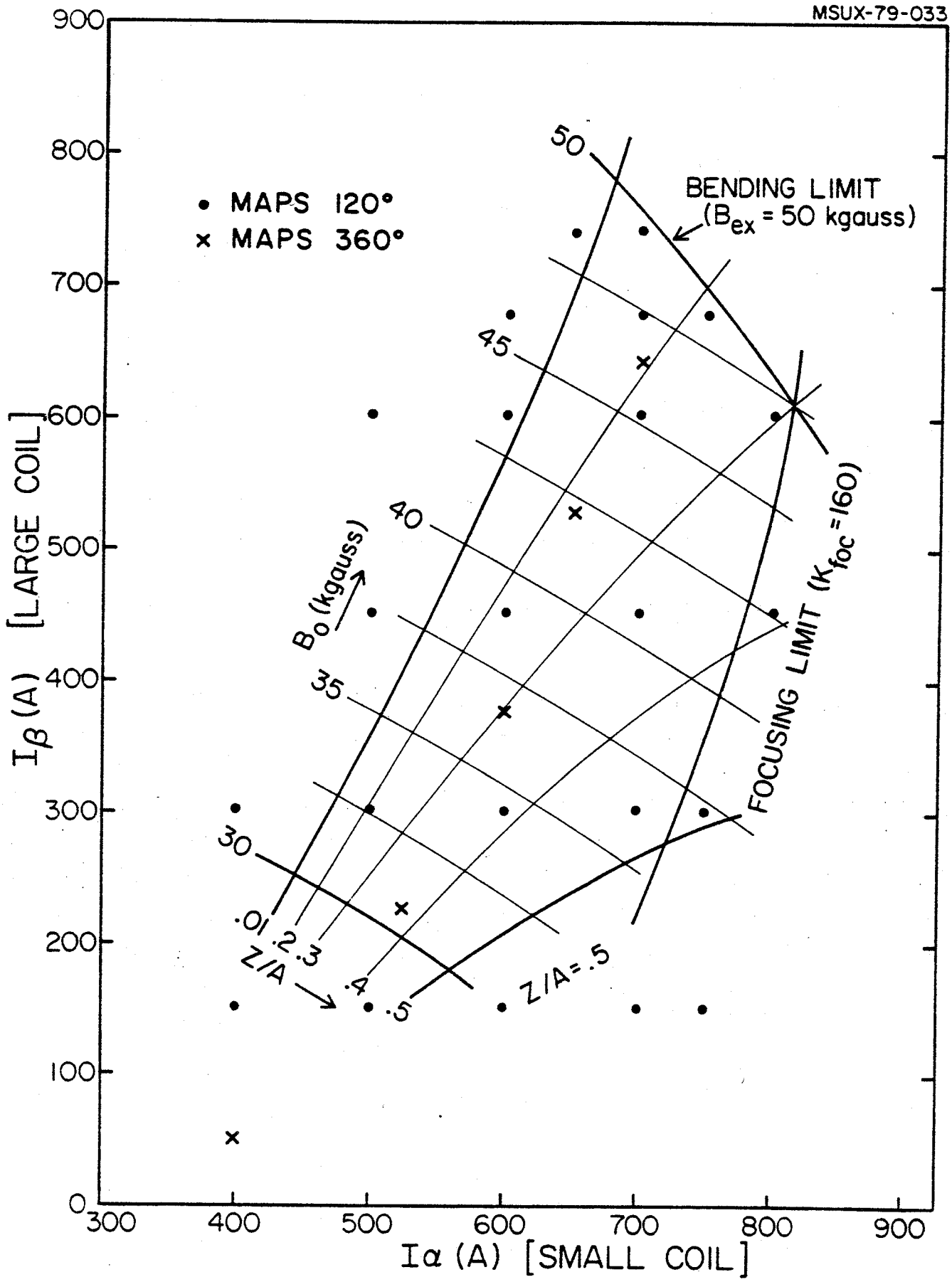

FIG. 8. Operating diagram of the K-500 cyclotron in the (I_α,I_β) plane. Also indicated are the measured maps.

by fitting (with a least squares procedure) the isochronous field as described in (2). As apparent from Fig. 8, the cyclotron is expected to operate for center field values, B_o, between 30 and 50 kgauss, and ions of charge to mass ratio Z/A between 0.01 and 0.5. The operating diagram is bounded by the bending limit, i.e. K=500 corresponding to a maximum field at the extraction radius B_{ex}=50 kgauss, and the focusing limit, i.e. T/A (MeV/n) = $K_{FOC} \cdot (Z/A)$ with K_{FOC}=160. A grid of lines with constant B_o and Z/A values is also shown.

The selection of the mapping points over the (I_α, I_β) diagram follows the criterion to have a grid as regular as possible in order to allow a precise interpolation for any intermediate point on the diagram. Limits posed by the maximum current at which the coils could be safely excited were also taken into account. The chosen grid is shown by dots on the diagram of Fig. 8. It consists of 23 points, the relevant I_α and I_β values being listed in Table I. Since the main goal of these maps was to study the field modulation and average field variations, they were taken over 120° only. It will be noted from Table I that the max. current for the small coil is 800 A, corresponding to an average density of 3900 A/cm^2. Two maps also required 740 A in the large coil. Although the coils had been designed[5] for a max. current of 700 A, no problems were encountered.

Table I. Data of 120° maps.

N	I (A)	I (A)	B_o (kgauss)	N	I (A)	I (A)	B_o (kgauss)
1	400	148	26.5	13	700	448	41.2
2	500	148	28.6	14	800	448	43.1
3	600	148	30.7	15	500	598	41.7
4	700	148	32.7	16	600	598	43.5
5	750	148	33.6	17	700	598	45.4
6	400	298	31.1	18	800	598	47.3
7	500	298	33.1	19	600	673	45.7
8	600	298	35.1	20	700	673	47.5
9	700	298	37.0	21	750	673	48.4
10	750	298	37.9	22	650	738	48.4
11	500	448	37.4	23	700	738	49.3
12	600	448	39.3				

Five 360° maps were also taken, as shown by the crosses in Fig. 8. Their main purpose was to check the field imperfections but at the same time they tested the reliability of the interpolation method used for predicting fields anywhere on the operating diagram.

4. Analysis of the azimuthal field modulation

4.1 Experimental Data

In the following the customary Fourier expansion of the magnetic field will be used, namely

$$B(r,\theta) = \bar{B}(r) + \sum_n C_n(r) \cos n\,(\theta - \phi_n(r))$$

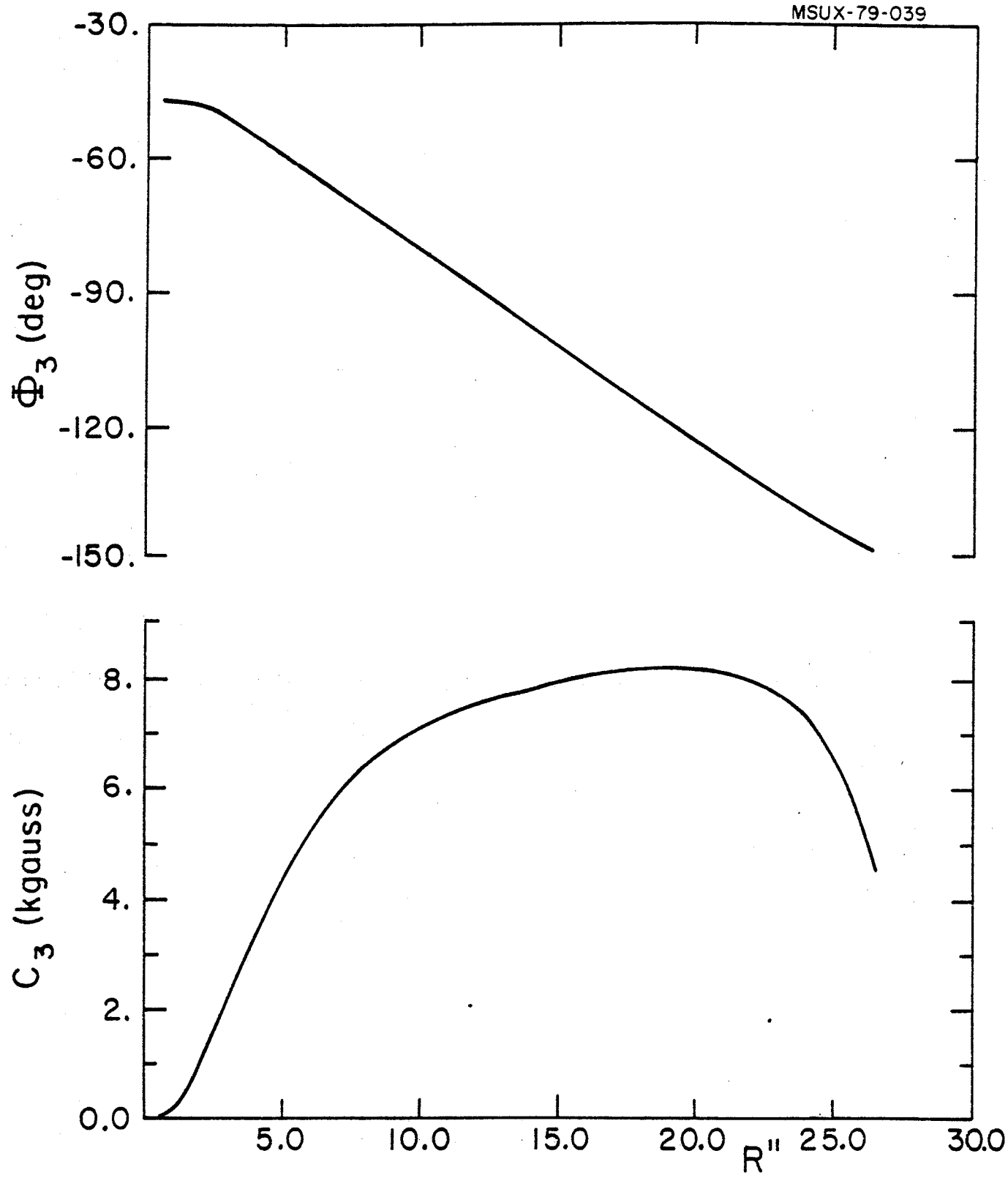

FIG. 9. Amplitude and phase of the 3rd harmonic, as a function of the radius, measured at I_α=700 A, I_β=298 A.

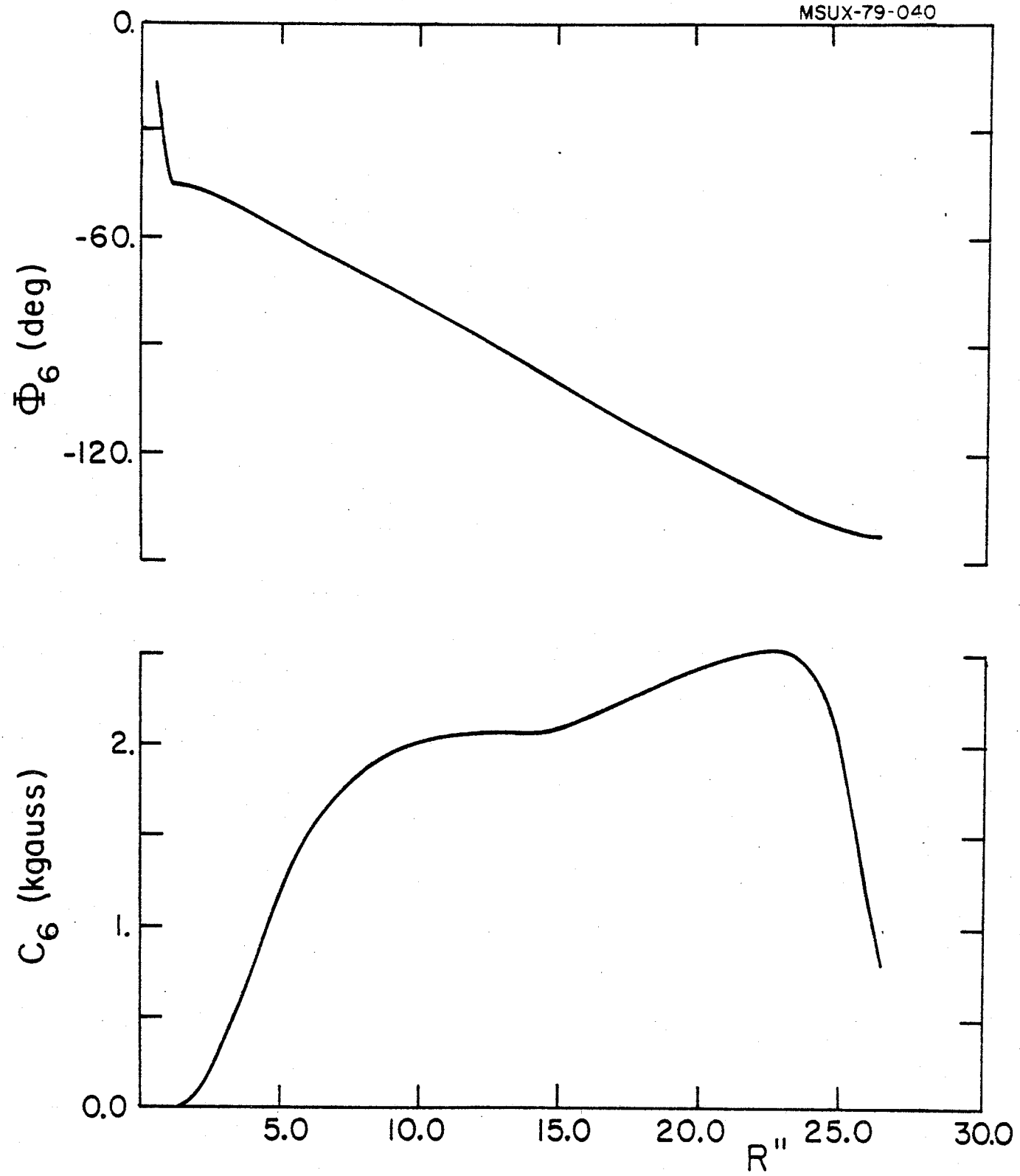

FIG. 10. Amplitude and phase of the 6th harmonic, as a function of the radius, measured at I_α=700 A, I_β=298 A.

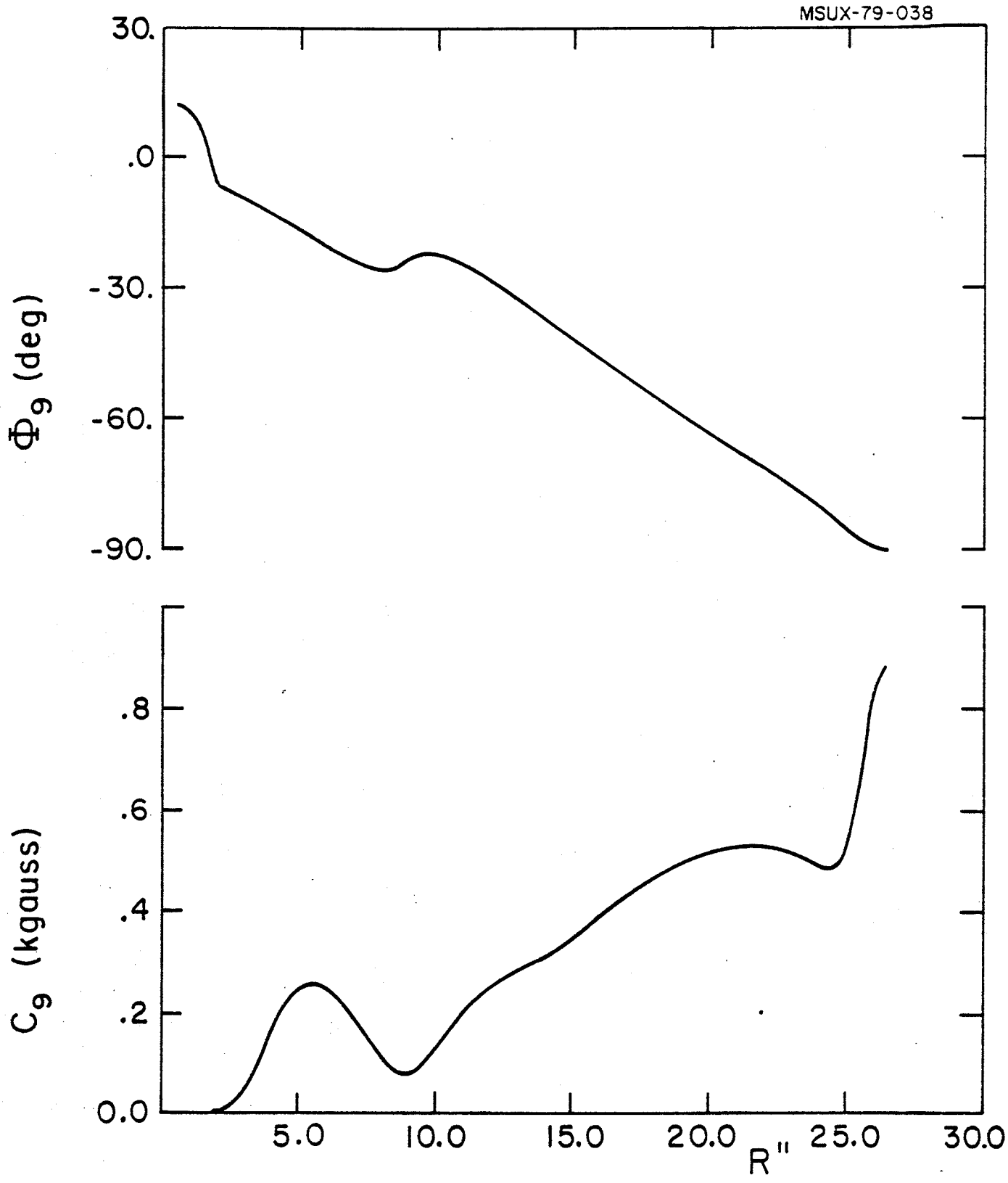

FIG. 11. Amplitude and phase of the 9th harmonic, as a function of the radius, measured at I_α=700 A, I_β=298 A.

where $\bar{B}(r)$ is the average field as a function of radius and the C_n are the harmonic amplitudes. For 120^o maps only the third harmonic and multiples thereof are present.

The 3^{rd}, 6^{th}, and 9^{th} harmonics are plotted as a function of the radius in Figs. 9, 10, and 11, both in amplitude and phase, for the map with I_α=700 A, I_β=298 A. Some features of the pole geometry emerge from a glance at the 6^{th} and especially the 9^{th} harmonics. In particular the 9^{th} harmonic exhibits a steep rise around or after 25", due to the 60^o wide hill shoes (from 26" to 27" in radius), and a bump between 4" and 10", accompanied by a phase shift, due to the first valley shim (see Fig. 2). Also noticeable, although to a much lesser extent, are the effects of the dee stem holes in the valley, centered at 16". The harmonic amplitudes, in the region of the maximum, (radii of 17" to 22") are very much proportional to the inverse of the square of the harmonic number.

Since the pole tips should be fully saturated at these field levels (30 to 50 kgauss), the harmonic amplitudes should not vary, in principle, at the different coils excitations. Small variations are however observed, with a rather suprising pattern. This is seen in Figs. 12 to 16, where the amplitude C_3 of the 3^{rd} harmonic at different radii is plotted as a function of I_α for fixed values of I_β. The radii are 10", 15", 20", 24" and 25", in this order, for Figs. 12 to 16. Some interesting features emerge from these plots:

- the dependence of C_3 upon I_α is very nearly linear, for any given value of I_β, and at all radii. It encompasses a maximum range of 100 gauss, i.e. about 1.5%.

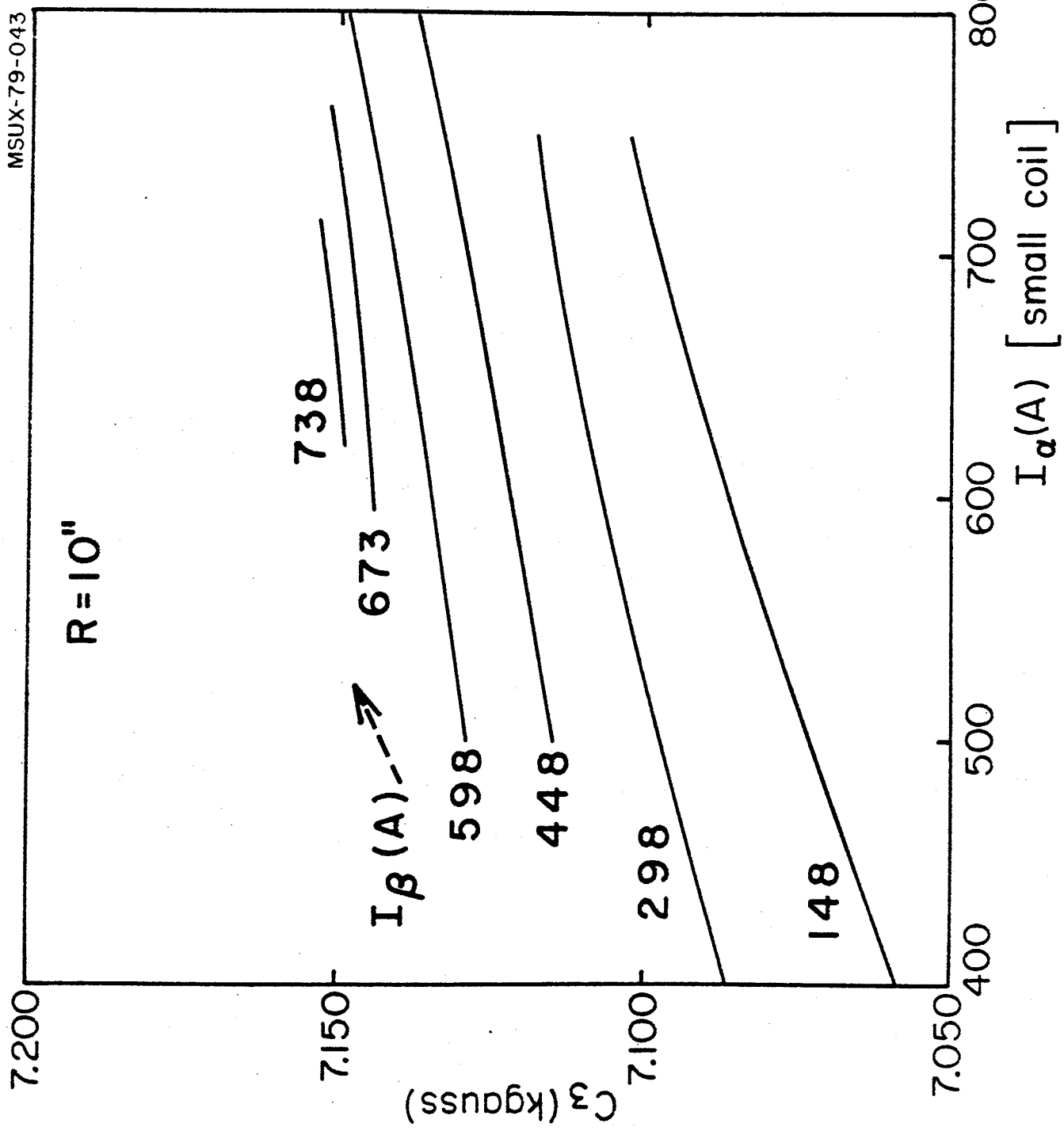

FIG. 12. Measured 3rd harmonic amplitude at a radius of 10" as a function of I_α for fixed values of I_β.

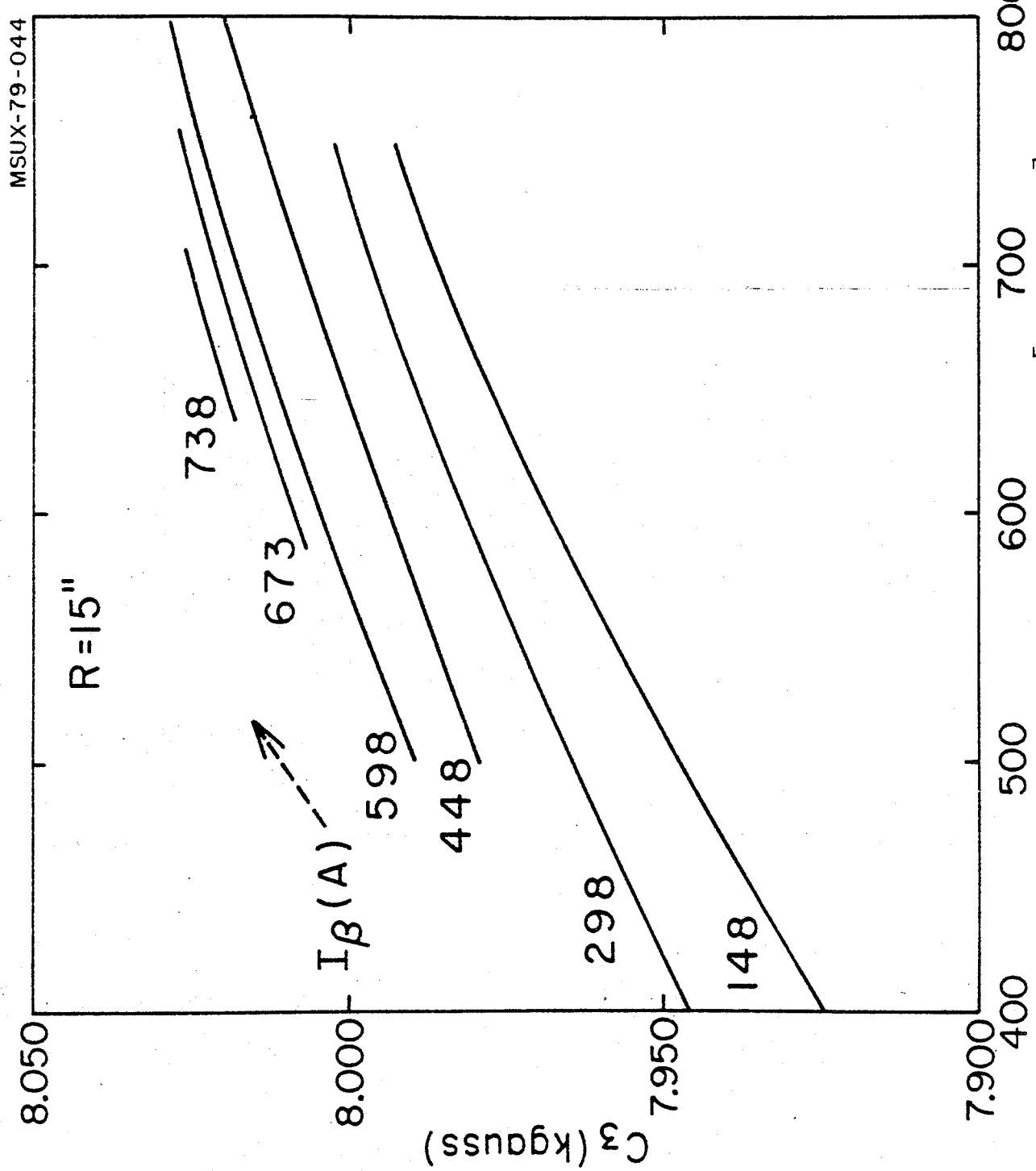

FIG. 13. Measured 3rd harmonic amplitude at a radius of 15" as a function of I_α for fixed values of I_β.

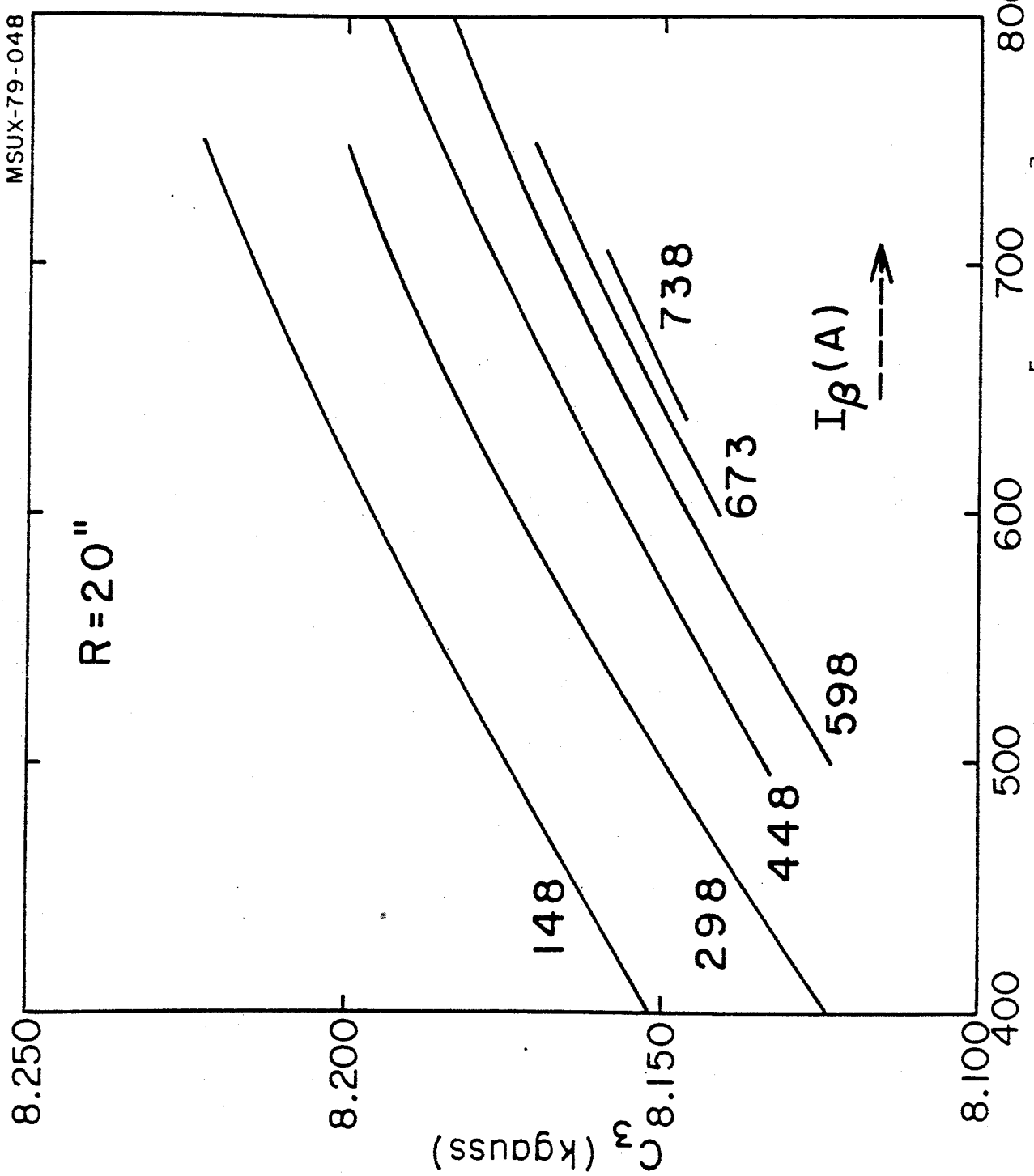

FIG. 14. Measured 3rd harmonic amplitude at a radius of 20" as a function of I_α for fixed values of I_β.

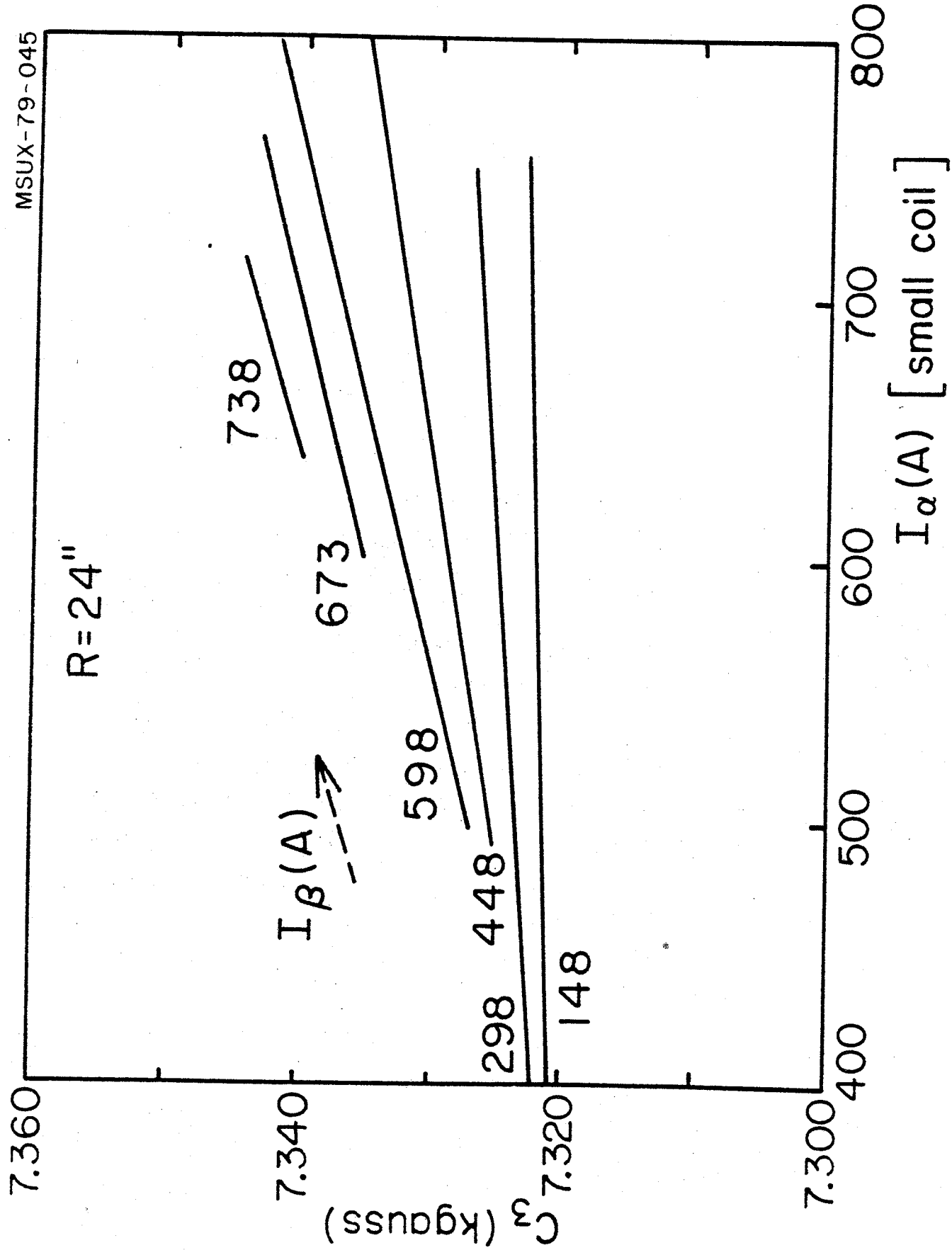

FIG. 15. Measured 3rd harmonic amplitude at a radius of 24" as a function of I_α for fixed values of I_β.

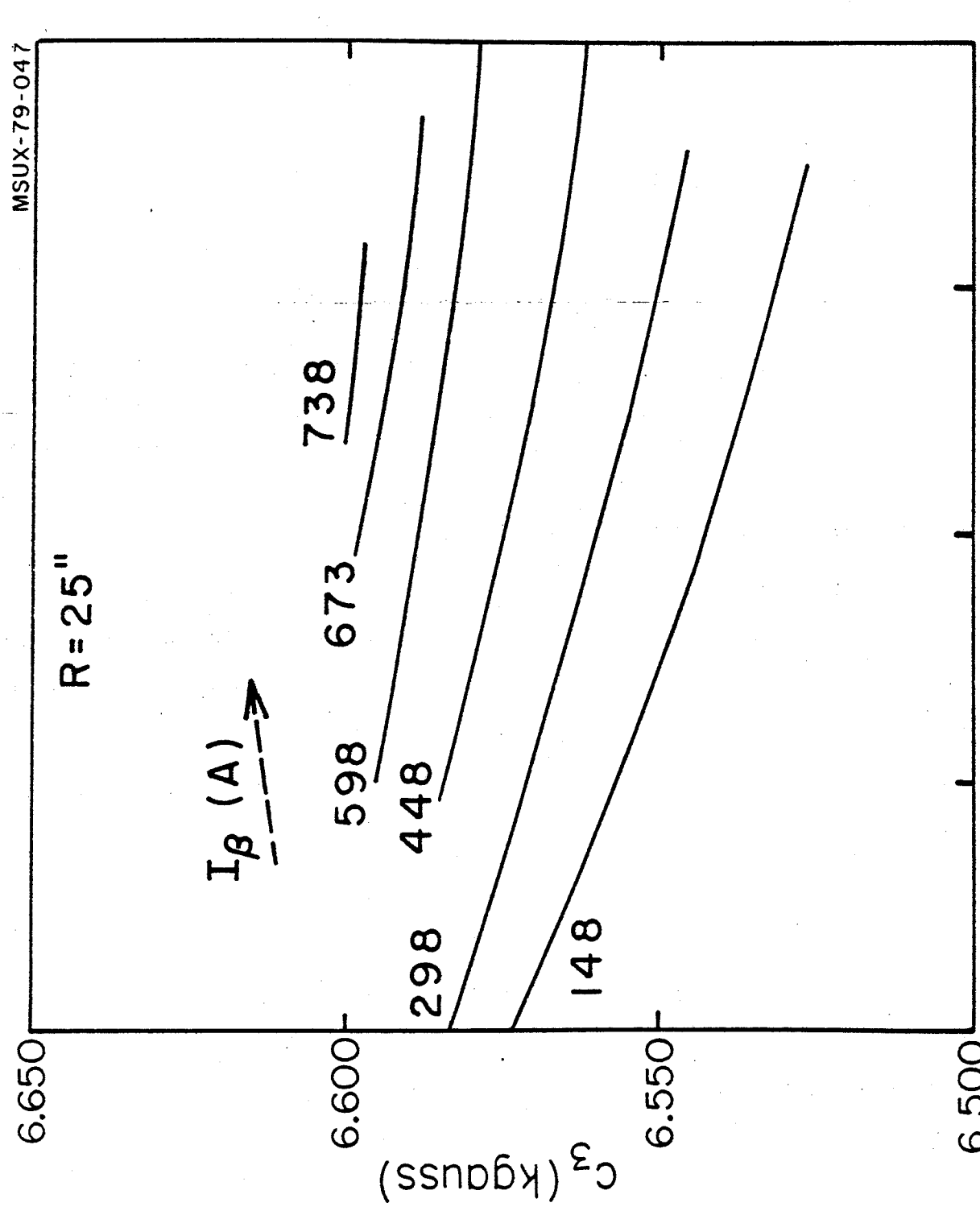

FIG. 16. Measured 3rd harmonic amplitude at a radius of 25" as a fucntion of I_α for fixed values of I_β.

- looking at Fig. 12, i.e. at 10" radius, it is seen that the maximum amplitude is obtained for the maximum of $(I_\alpha + I_\beta)$ and the minimum at the minimum of such sum. This pattern also persists at 15", Fig. 12.
- a "reversed" trend is then observed in the radial region from 17"-17.5" to 23"-23.5". An example of this is shown in Fig. 14 at 20" radius, where the maximum C_3 is obtained for I_β=148 A, and the minimum for I_β=738 A. The slope of the lines is essentially the same as at 15". The region of 17" to 23" coincides, see Fig. 9, with the flat maximum of the amplitude as a function of radius.
- at 24" radius, Fig. 15, the trend is back to normal. Note however the difference in scale of Fig. 15 with respect to the previous ones and the sizable difference in the slope, which is much flatter.
- at 25" radius, Fig. 16, the trend is normal, but the slope is now reversed, i.e., the harmonics amplitude decreases with increasing I_α. It should be noted that beyond 23" the third harmonic amplitude starts decreasing rapidly (see Fig. 9).

4.2 Comparison with calculations

The only practical way to calculate the azimuthal field modulation arising from a geometry as complex as the present one is by supposing the pole tip surfaces to be fully saturated with the magnetization M aligned with the Z-axis.

This technique has been known to yield excellent results[6,7] but gives of course a fixed azimuthal modulation, in contrast to the data reported above. In view of those we compare the calculations with the data at an excitation I_α=700 A, I_β=298 A. The reason for this choice is that this is about the excitation needed to reach K_{FOC}=160 for Z/A=.5 ions, as seen from Fig. 8. Consequently the axial focusing, stemming from the field modulation, is more critical.

This comparison is presented in Fig. 17 for the 3^{rd}, 6^{th} and 9^{th} harmonics, which shows the calculated values somewhat higher than the experimental ones. The calculated values refer to a saturation magnetization M=21.4 kgauss. For the 3^{rd} harmonic, and at the same coils excitation, a more precise idea of the discrepancy can be seen in Fig. 18, where the percentage difference between calculated and measured C_3 is plotted as a function of radius. Very similar results are found at all other coils excitations. The peculiar behavior of the curve obviously suggests that more than just a different value of the iron magnetization is involved.

Let us first note that the observed range of discrepancy, up to 3%, is larger than the measured variations caused by the different coil excitations (1.2% or in fact $\pm$ .6% at the chosen excitation of I_α=700 A, I_β=298 A).

The discrepancy peaks at a radius of 14", which coincides with the splitting of the pole tips mentioned before. A similar trend is observed after 22", in proximity to the 1/4" discontinuity of the hill structure, located at a radius of 25.75". It seems unlikely that geometrical differences like the actual

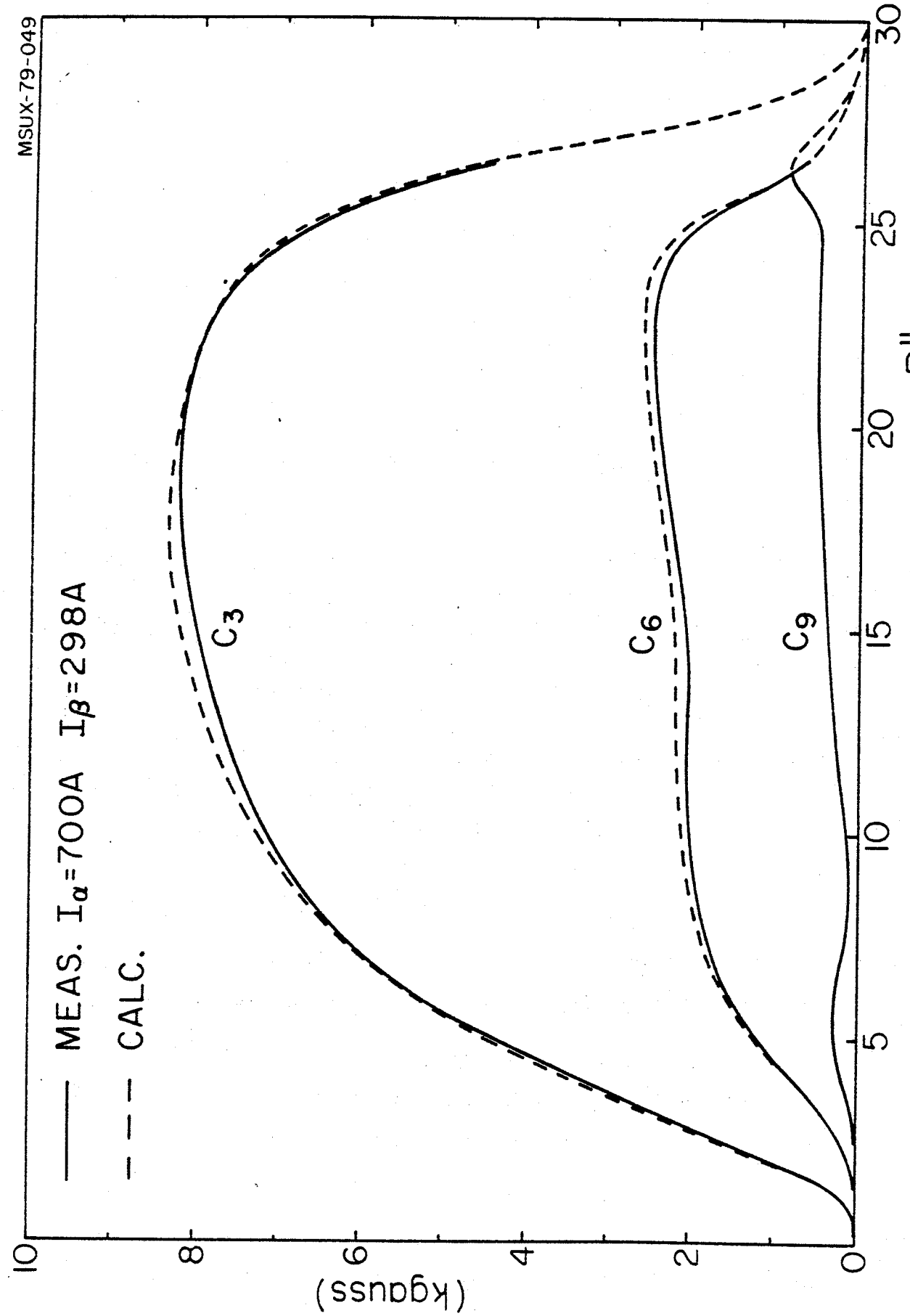

FIG. 17. Measured and calculated amplitude of the 3rd, 6th and 9th harmonic, as a function of the radius, at the listed coil currents.

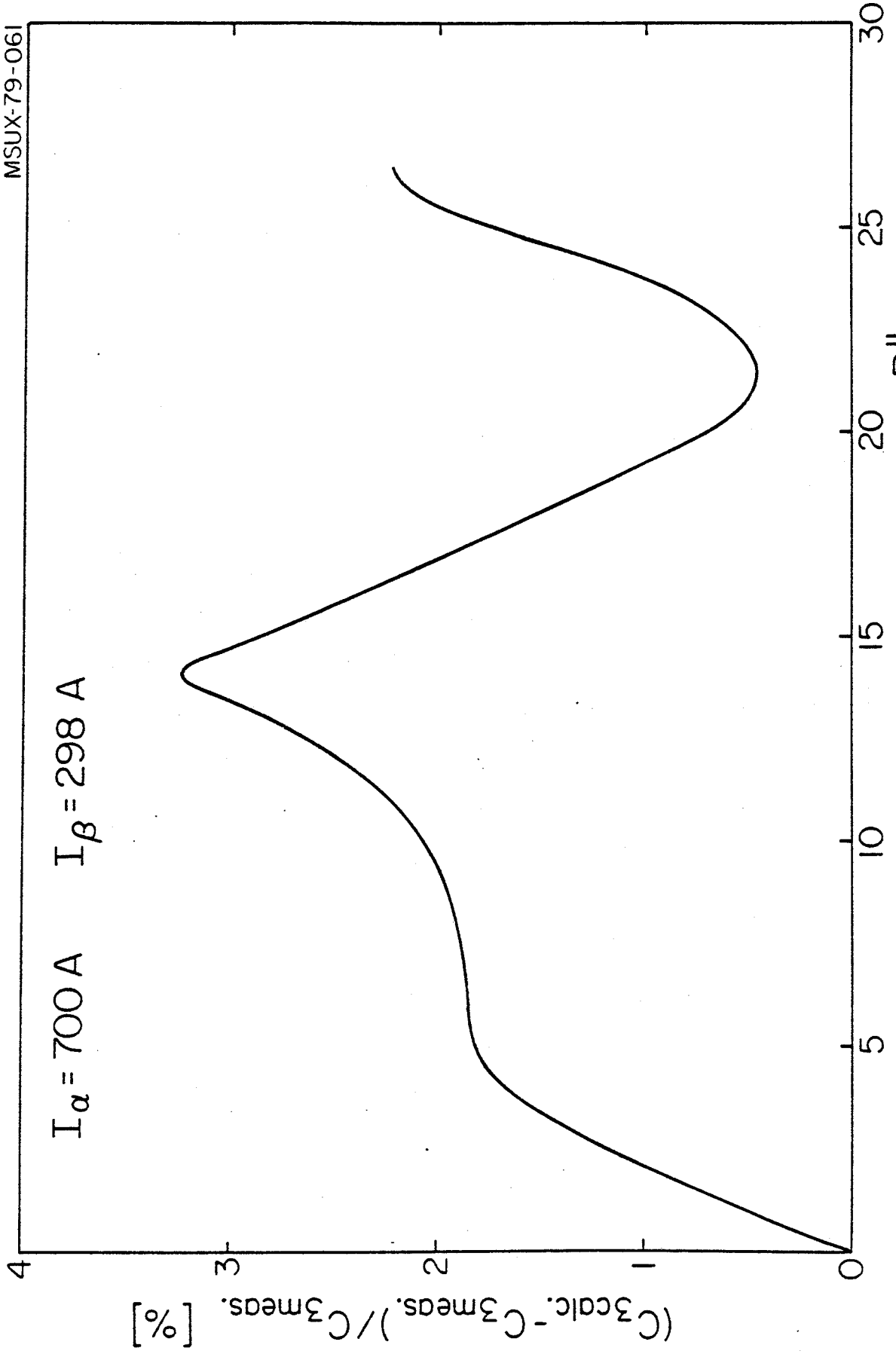

FIG. 18. Percentage difference between measured and calculated amplitude of the 3rd harmonic as a function of the radius.

hill width vs. the calculated one are responsible for these effects, as well as for the shallow minimum of Fig. 18. The latter is centered around 20" and stretches roughly over the same radial region where the "reversed" trend of C_3 with (I_α, I_β) is observed. Although we have no firm model for the observed variations of the harmonic amplitudes, it is likely that the coil generated field and more particularly its topography (i.e. the behavior of the field lines of force) have a definite influence on the local saturation both in strength and direction.

One should also keep in mind that the valley profile, as shown in Fig 2, does have pronounced discontinuities, like the presence of the dee stem hole and the sharp edge of the shim at a radius of 22", where the valley floor drops from 11" to 18" with respect to the median plane. It is likely that in these regions the approximation of a uniform saturation with M parallel to the z-axis fails to some extent.

As a conclusion, even though the uniform saturation hypothesis is adequate to design a superconducting cyclotron, discrepancies of 2%-3% are not really negligible. Since the calculated values are higher, the observed discrepancies imply an effective flutter reduction of 4%-6% and therefore a corresponding reduction in the axial focusing. Some margin should therefore be allowed for, when designing such cyclotrons. These results could conceivably be different for different coil and magnet geometries.

5. Analysis of the average magnetic field

Since the coil-produced field can be calculated exactly, we can write $\bar{B}(r,I_\alpha,I_\beta) = \bar{B}_{iron}(r,I_\alpha,I_\beta) + B_{coils}(r,I_\alpha,I_\beta)$ and confine our analysis to the iron generated field. Let us note that $\bar{B}_{iron}(r)$ would not be a function of (I_α,I_β) if it were generated only by a saturated dipole distribution on the pole tips. In fact the contribution from the variable saturation of the yoke is quite important and affects both the absolute level and the average slope of $\bar{B}_{iron}(r)$. We shall first review the experimental data and then compare them with calculations.

5.1 Experimental data

As noted before, the data of the maps are limited to an outer radius of 26.5", dictated by the tank inner wall. Since this radius coincides roughly with the extraction radius of the cyclotron, the knowledge of the magnetic field that far is adequate for the study of the internal beam dynamics up to extraction.

This is however a definite need to know, although with lesser precision, the fringing field in order to calculate with some accuracy the path of extracted beams. Since the comparison of the data with calculations, described in the following, indicates that discrepancies up to a few hundred gauss may be present, one should not rely on calculations alone. Fringing field measurements were carried out by inserting the flip coils bar through a radial hole existing in the median

plane of the cryostat. Data were therefore taken at .5" radial intervals at a fixed azimuth, and at the same coil excitations used for the internal maps. In order to extract average field values from these data, the calculated field harmonics were matched in phase and amplitude to the measured ones at the radius of 26.5" by multiplicative scaling. The new harmonics thus calculated at all radii larger than 26.5" were used to subtract from the measured data the field modulation corresponding to the relevant azimuth, therefore obtaining an average field for any given radius.

This average field is obviously affected by errors in the harmonics amplitude, which may be of the order of a few percent in spite of the matching procedure. However, since at a radius of 28" the C_3 value is already down to 1 kgauss, and is between 200 and 100 gauss from 30" to 40", the resulting errors are quite tolerable. We estimate the accuracy of the average fields deduced in this way at radii larger than 26.5" to be $\pm$ 40 gauss up to 30" and $\pm$ 15 gauss afterwards.

The measured $\overline{B}_{iron}$ (r) are plotted in Fig. 19, for six typical coil excitations, which encompass the whole operating range of the cyclotron. The values of the total magnetic field at the center, B_o, are also listed for reference. One can remark that the center value of $\overline{B}_{iron}$ varies by about 3 kgauss, from 16.2 to 19 kgauss, in going from the minimum to the maximum field. There is also a definite change in slope, the slope increasing with the average field values, thus pointing out that the $\overline{B}_{iron}(r)$ increases more rapidly at inner radii than at the outer ones. The cone field up

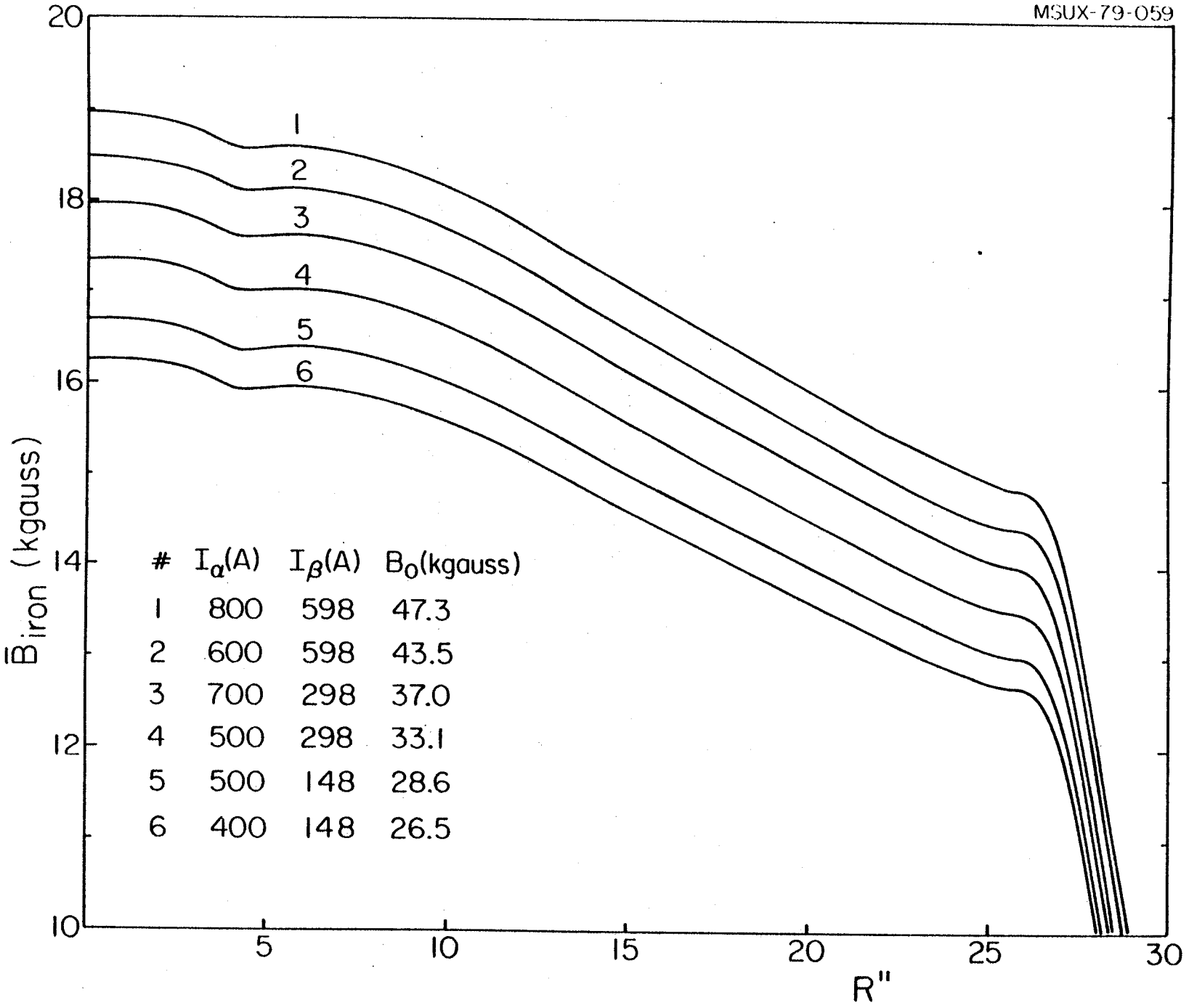

FIG. 19. Measured average iron field, as a function of the radius, for the listed coil currents. B_o represents the total field measured at the center.

to a radius of 3.5"-4", produced by the center plug, is quite evident.

The change in values and slope of $\bar{B}_{iron}(r)$ is more readily appreciated in Fig. 20, where the values of $\Delta\bar{B}_{iron}(r,I_\alpha,I_\beta) = \bar{B}_{iron}(r,I_\alpha,I_\beta) - \bar{B}_{iron}(r,400,148)$ are plotted for five different (I_α,I_β) values. The zero line corresponds therefore to the $\bar{B}_{iron}(r)$ at the excitation I_α=400 A, I_β=148 A, i.e., the one at minimum total field (B_o=26.1 kgauss) in our mapping range. The maximum change in slope thus occurs at the highest excitations and is as high as 500 guass if calculated between 0" and 26.5".

Non-linear effects are seen in the fringing field region between 25" and 30". They are of the order of 100 gauss, after allowing for the possible errors in the fringing field measurements, pointing out that at the magnet edge the influence of the different coil excitations plays a substantial role in shaping the iron-produced field. A plot of the fringing field at three different excitations and between 24" and 42" is shown in Fig. 21. The details of the tank walls and the coil location are also schematically indicated. Again very sharp non-linear effects, are seen in the proximity of iron structures (inner and outer coil tank walls). Possible sources of error in the fringing field region related to the coils field contribution will be discussed later.

The measured variation of $\bar{B}_{iron}(r)$ as a function of I_α, and for fixed I_β values, is presented in Figs. 22, 23, 24, at the radii of 10", 20" and 25" respecitvely.

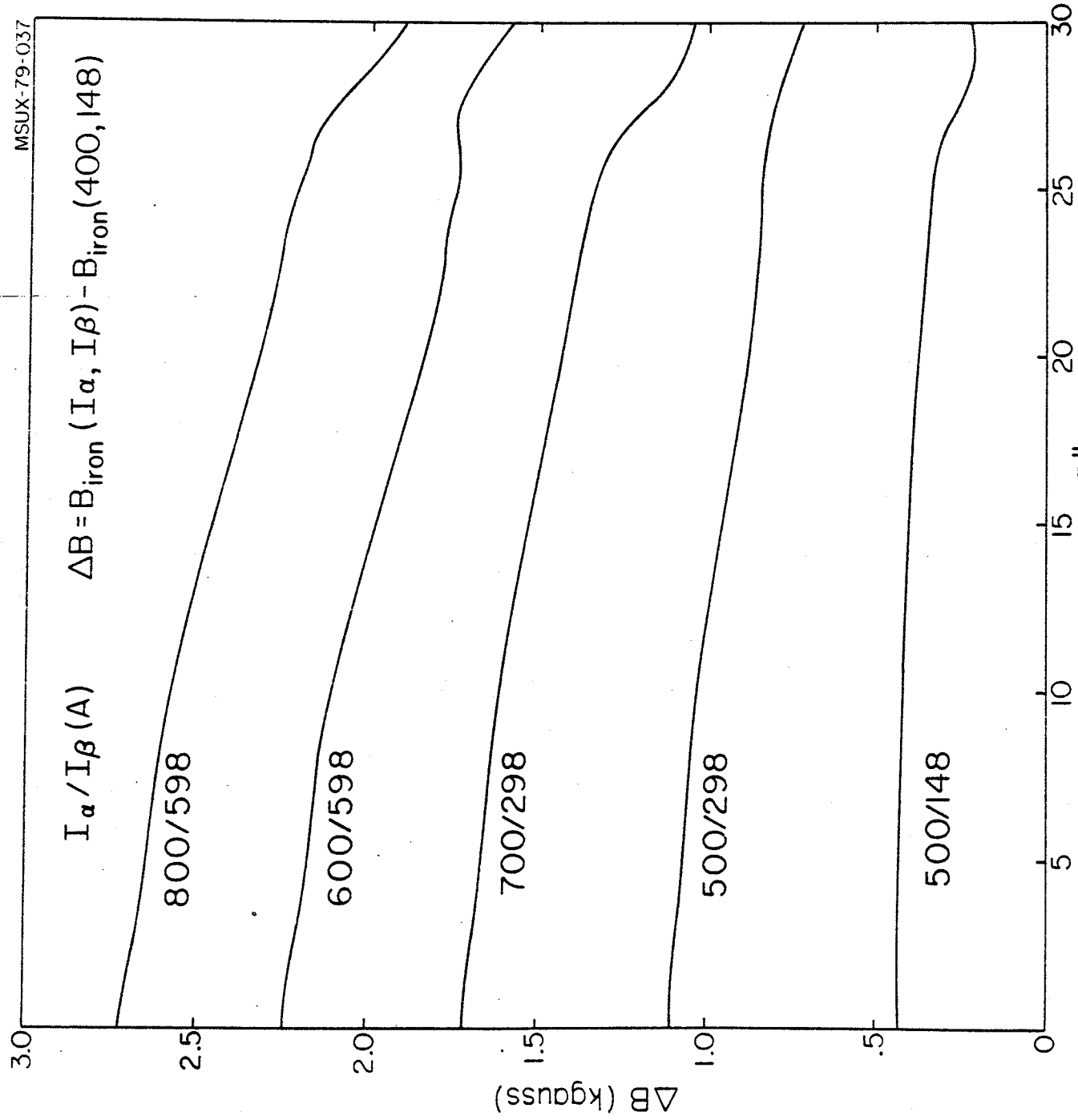

FIG. 20. Measured average iron field variation for the listed coil currents respect to the field at I_α=400 A, I_β=148 A.

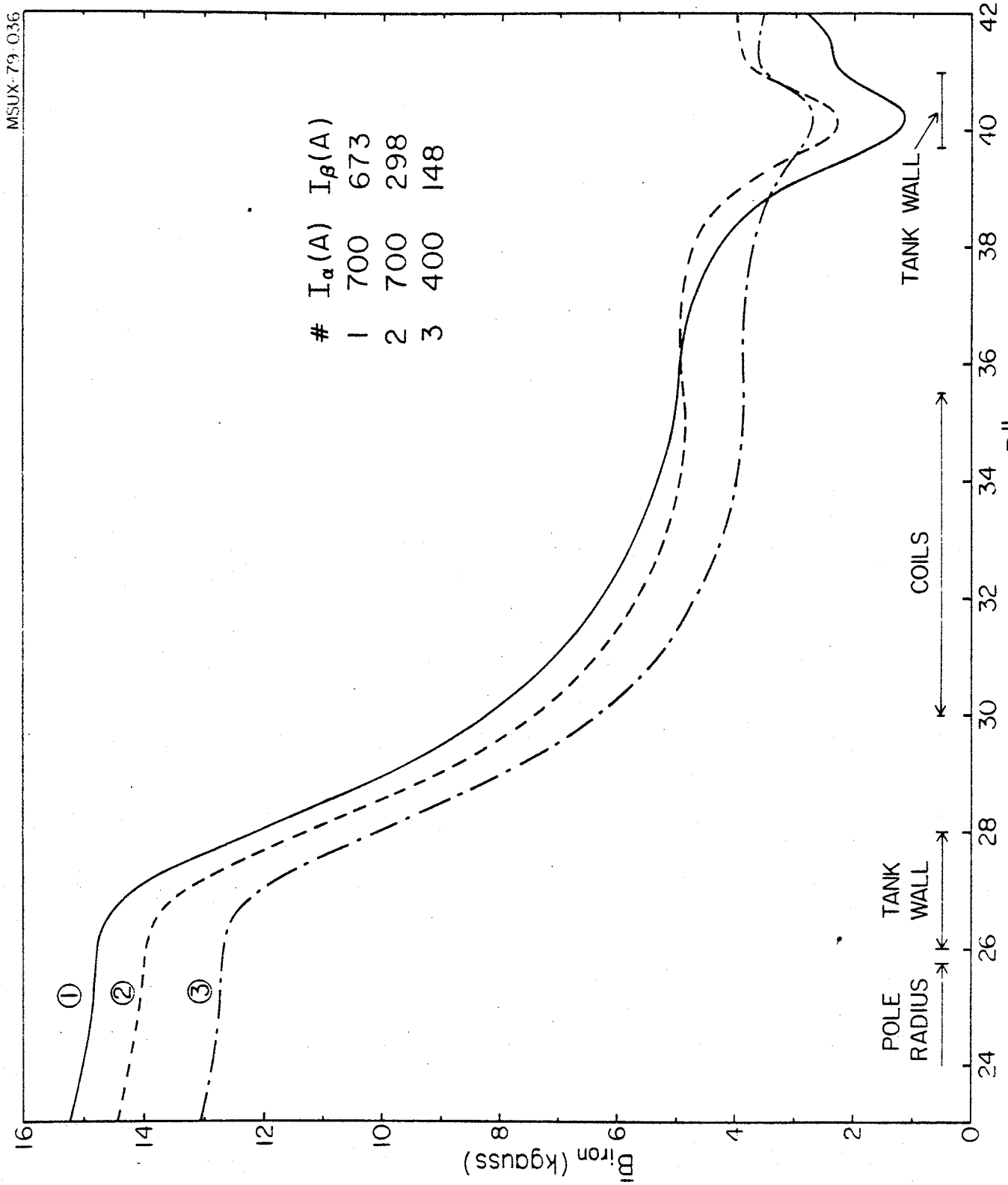

FIG. 21. Average iron field, as a function of the radius, for three different coil currents.

The plots are almost linear, as expected, with some deviation from linearity being most pronounced, at all three radii, for the I_β=148 A line. No "reverse" trend, as observed for the azimuthal modulation, is found. All attempts to parametrize the observed variation of $\bar{B}_{iron}(r)$ at any given radius, in terms of just one parameter, like the total number of ampere-turns in the two coils section, or the total average field value, or even the total magnetic flux in the poles have failed. As an example, Fig. 25 shows the values of $\bar{B}_{iron}$ at 20", for all 23 maps, as a function of the total number of ampere-turns. The lines delimiting the band are just a guide to the eye. Typically, for the same number of ampere-turns but different (I_α, I_β) settings field values differing by as much as 400-500 gauss are observed, with a tendency to a reduction of the spread at the highest excitations where some yoke saturation is slowly approached. It is clear therefore that the relative excitations of the coil sections play again an important role in the level and shape of the iron produced field.

5.2 Comparison with calculations

Since exact three-dimensional calculations are not possible, one way to calculate the $\bar{B}_{iron}(r, I_\alpha, I_\beta)$ is to use one of the existing codes for cylindrical symmetry problems, and develop a model which simulates the inherent 3-dimensional geometry.

This has been done in our case, by using the code TRIM[8] and the model which is summarized in the following.

The basic idea underlying the model is to replace all non circularly symmetric structures, i.e. hill, shims, holes,

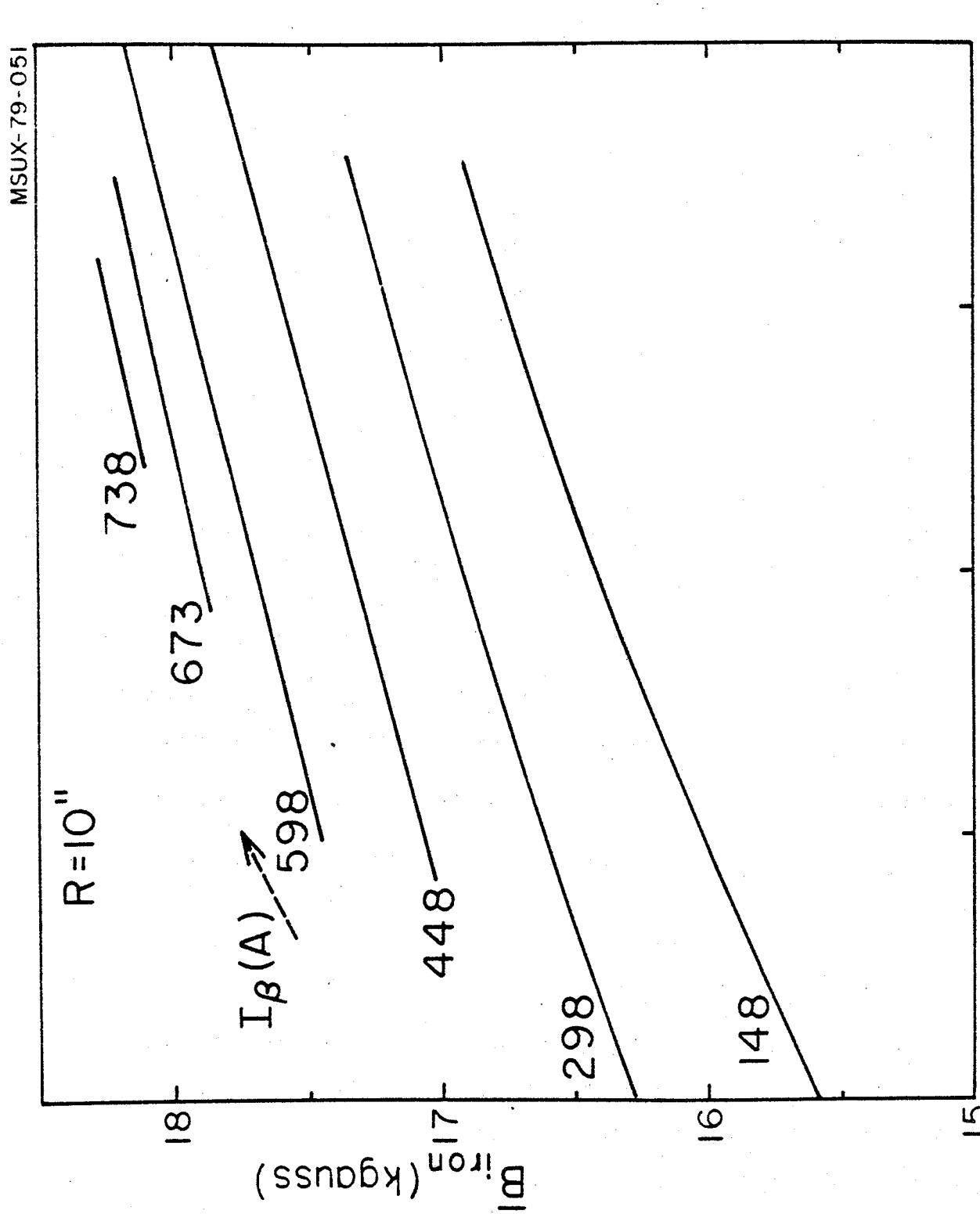

FIG. 22. Measured average iron field at a radius of 10" as a function of I_α for fixed values of I_β.

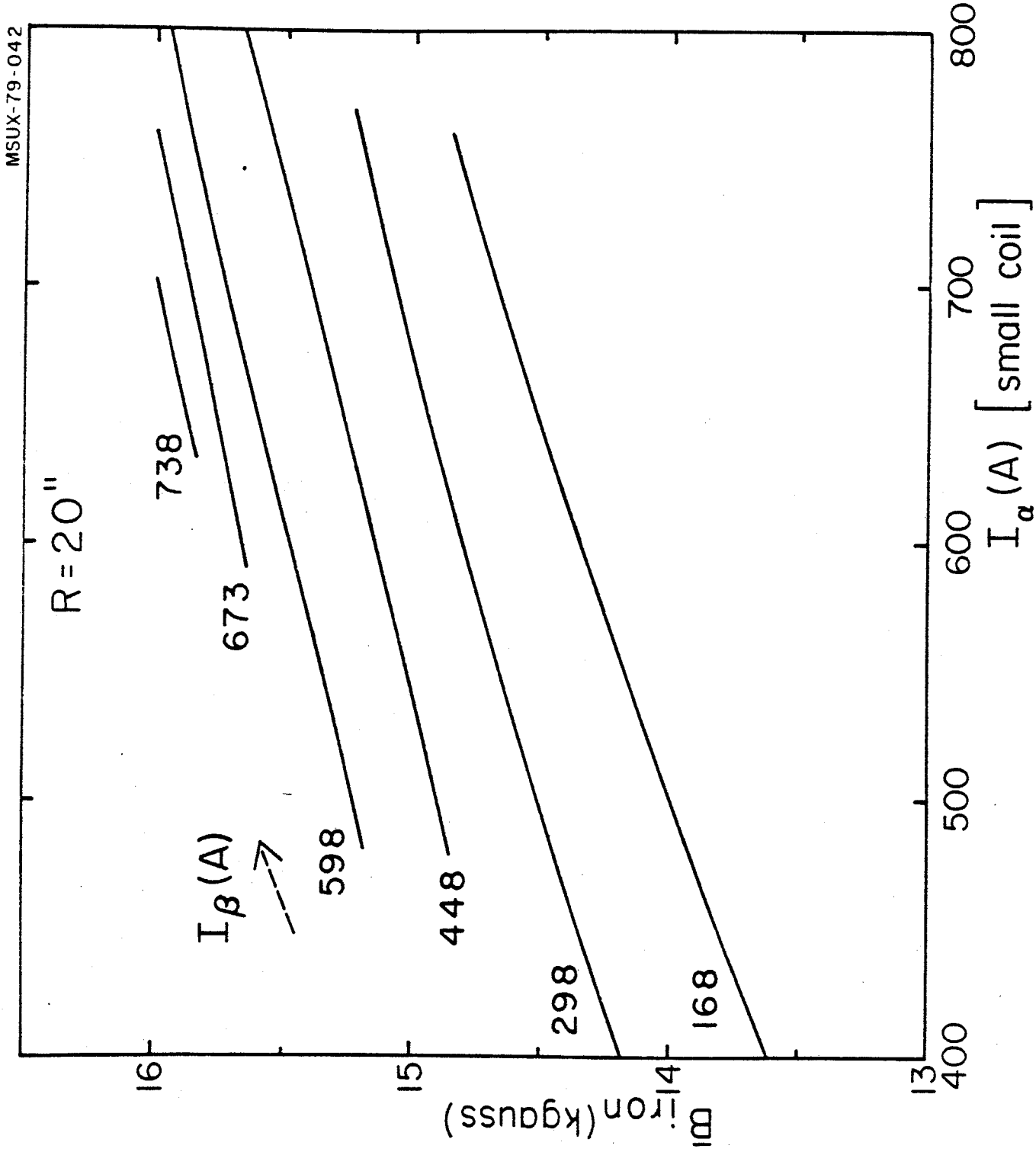

FIG. 23. Measured average iron field at a radius of 20" as a function of I_α for fixed values of I_β.

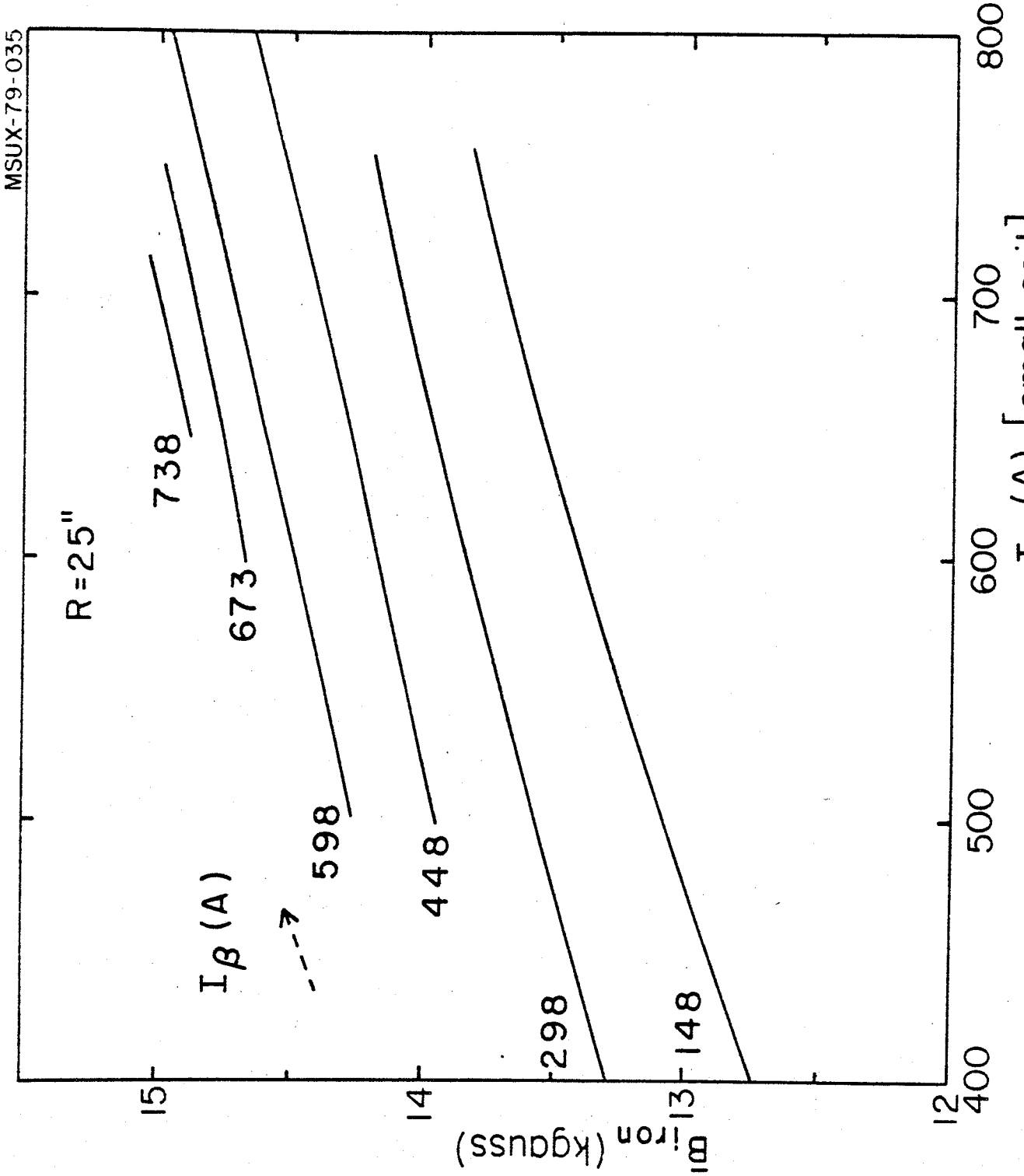

FIG. 24. Measured average iron field at a radius of 25" as a function of I_α for fixed values of I_β.

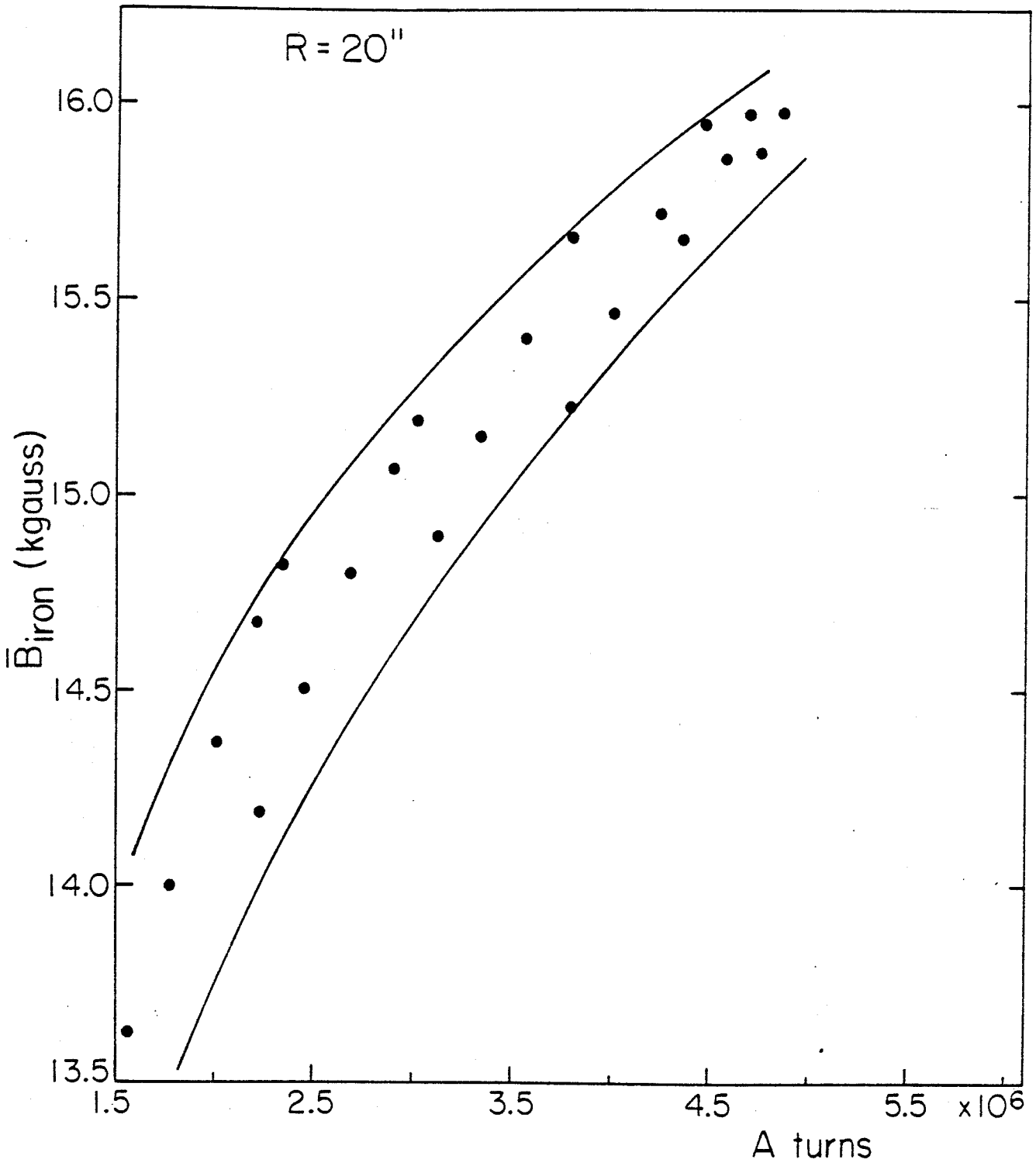

FIG. 25. Measured average iron field at a radius of 20" as a function of the total number of Ampereturns in the coils.

etc. by rings of equal or equivalent dimensions whose permeability is reduced with respect to that of the iron regions with cylindrical symmetry. We assign therefore to these rings on iron fraction $0<F<1$, which accounts for the fact that in the actual geometry the volume they occupy is reduced by the intrinsic threefold symmetry.

Most of the pole and the coils dimensions are as in reality, as indicated in Fig. 26, which shows the actual TRIM grid. The outside yoke radius is 60", the max. height above the median plane being 43". The inner cryostat wall (r=26" to 28") and the clearance gap of .25" between pole tip and tank are also like the real magnet. The upper and outer tank walls, being of iron, have been combined with the yoke, giving a coil chamber height of 25.75" and an inner yoke radius of 41". The coil dimensions, r=30" to 35.6", Z=1.43" to 7.84" and Z=8.22" to 21.05", are like the real ones, with 1115 turns in the small coil and 2228 in the large one.

The dee stems holes are simulated by rings of inner radius 11.49" and outer radius 20.11", these values being selected as those at which the fraction of the ring cut by the holes drops to 1/2 the max. value. The actual holes, centered at a radius of 16" and with 10" diameter, remove a volume of iron equal to .276 of the ring so that the iron fraction used in computing the permeability is 1-.276=.724.

The pole tips are split into four ranges of lowered permeability. The hill shoe, already described, being 60° wide is represented by a ring of 0.5 iron fraction. The main parts

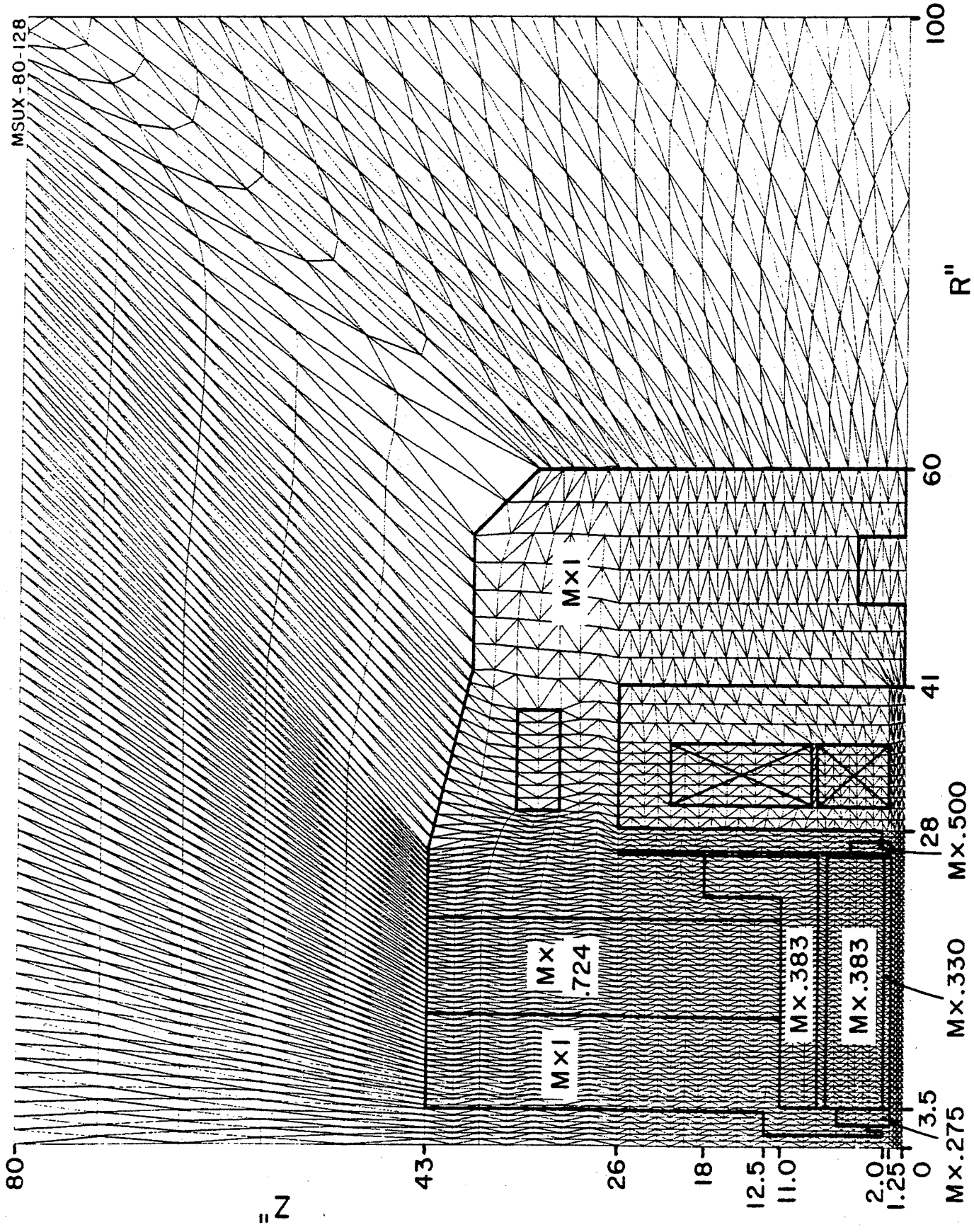

FIG. 26. Grid used in the program TRIM for the relaxation calculation of the magnetic field. See text for details.

of the hills are represented by two pieces of 0.383 iron fraction. This value is correct for a 46° hill width, and allows the valley floors (where the 100% iron begins) to be at the correct heights for radii greater than 10". The cut-off corners of the hills are accounted for by widening the trim coil return gap (Z=7.00 to Z=7.75") to 0.83" and by lowering the iron fraction to 0.330 in a layer between Z=1.25" and Z=1.85".

The iron fraction of .383 is too high for radii less than 10", where the hill approaches a 33° width. To get the same total volume of iron as the real magnet, the valley floor is changed from Z=9.25" to Z=11.0" (r=3.5"-10").

The cylindrical part of the plug is treated exactly, while the hill part of it is simulated by ring with iron fraction .275 which corresponds to a 33° width.

Also apparent in Fig. 26 are two iron-free regions respectively above the coils and in the yoke. The first one simulates the vertical holes in the yoke for the vertical coil support links, the coils leads and the helium and the nitrogen feeds. The second one simulates the horizontal holes around the yoke median plane which are needed for the radial coil support links, extraction elements etc.

For TRIM the iron is described by B vs. H tables, with B and H in gauss and oersteds, so that B/H=1 for air. The permeability for part-iron regions is assumed to be a weighted average of the values for air and iron:

$$(B/H)_F = F\,(B/H)_{1.0} + (1.0-F),$$

where F is the iron fraction. For each H in the original table, a new B is calculated:

$$B_F = F\ (B_{1.0}-H) + H$$

The TRIM runs for this magnet require 6 B vs. H tables, for iron fractions of 1.0, 0.724, 0.5, 0.383, 0.330 and 0.275.

For this model to be reliable the calculated average fields of the actual three-dimensional iron configuration and of the equivalent rings should coincide. Such a check can be carried out only in the uniform saturation approximation, which is an hypothesis well verified only for the surfaces close to the median plane.

This is actually carried out and the resulting difference between the fields of the equivalent rings and the real configuration (both calculated assuming M=21.4 kgauss but scaled down by the iron fraction for the relevant rings) is added to the TRIM computed fields. It should be pointed out that this difference is a constant for all coil excitations.

With this model a grid of 19 maps was run at I_α, I_β excitations close in most cases to the measured ones. An interpolation then provided the calculated average fields at precisely the same excitations as the measured maps, for a detailed comparison. It was checked that the interpolation is self-consistent and agrees with an actual calculation within 10-15 gauss.

The differences between the calculated and measured $\bar{B}_{iron}(r)$ values are presented in Fig. 27 for a fixed I_α of 700 A and different I_β values. Similar differences are presented

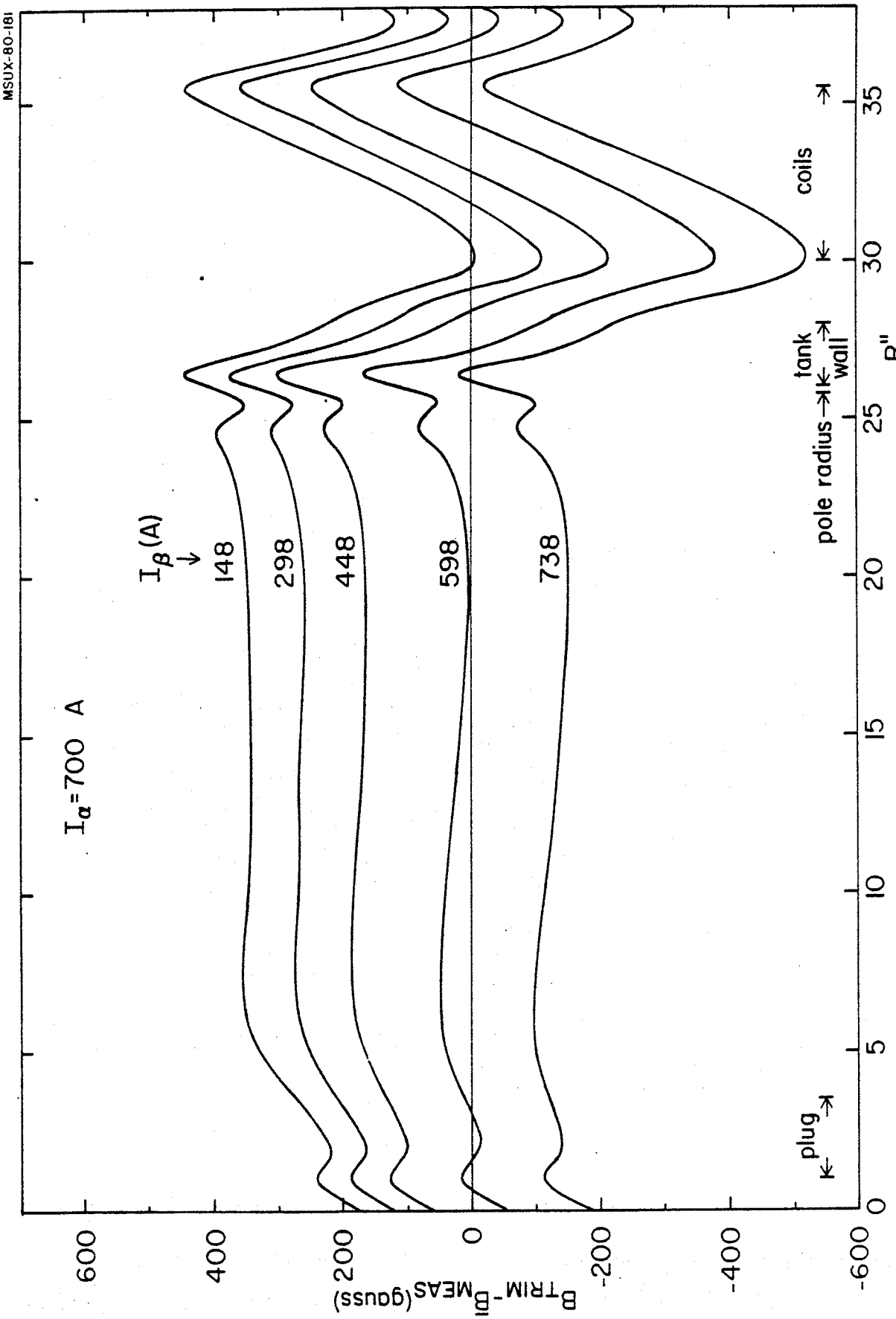

FIG. 27. Differences between calculated and measured iron field, as a function of the radius, for I_α=700 A and different values of I_β.

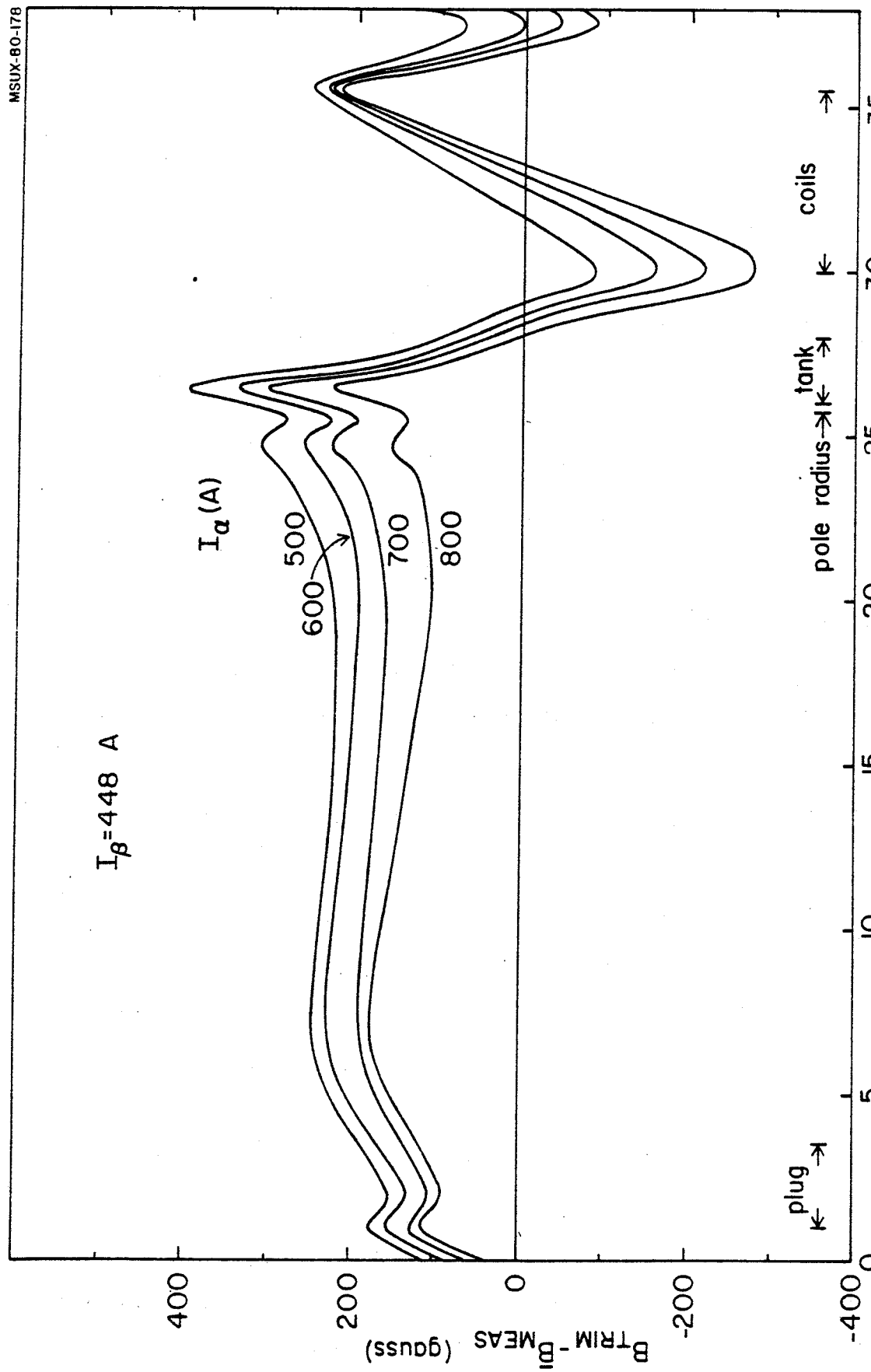

FIG. 28. Differences between calculated and measured iron field, as a fucntion of the radius, for I_β=448 and different values of I_α.

in Fig. 28 for a fixed I_β of 448 A and different I_α values. As a glance to Fig. 8 shows, these two figures correspond to two rather representative lines across the cyclotron operating range in the (I_α, I_β) plane.

The following features emerge:

- Oscillations are seen in the plug region and the pole edge region, with a rather constant pattern.
- At radii between 5" and 25" the most relevant error of the model is a field level error, while the slope seems essentially well reproduced.
- Very large oscillations are seen in the fringing field region, again with a pattern rather independent of the coils excitation.

Discussing first the oscillations near the plug and at the pole edge, we recall that in these regions discontinuities in the iron configuration are most pronounced. Insufficient detail of the TRIM description in these regions, due to the finite number of mesh points, is the most likely cause for the observed pattern.

Turning now to an analysis of the observed field level error in the radial range of 5" to 25", Fig. 29 presents the calculated $\bar{B}_{iron}(r)$ vs the measured one at a radius of 20". All the points corresponding to the 23 measured maps are shown and labelled differently according to their I_β currents. All points should lie on the dashed line in case of complete agreement. For the sake of completeness the numerical values of the observed differences are presented in Fig. 30 in the

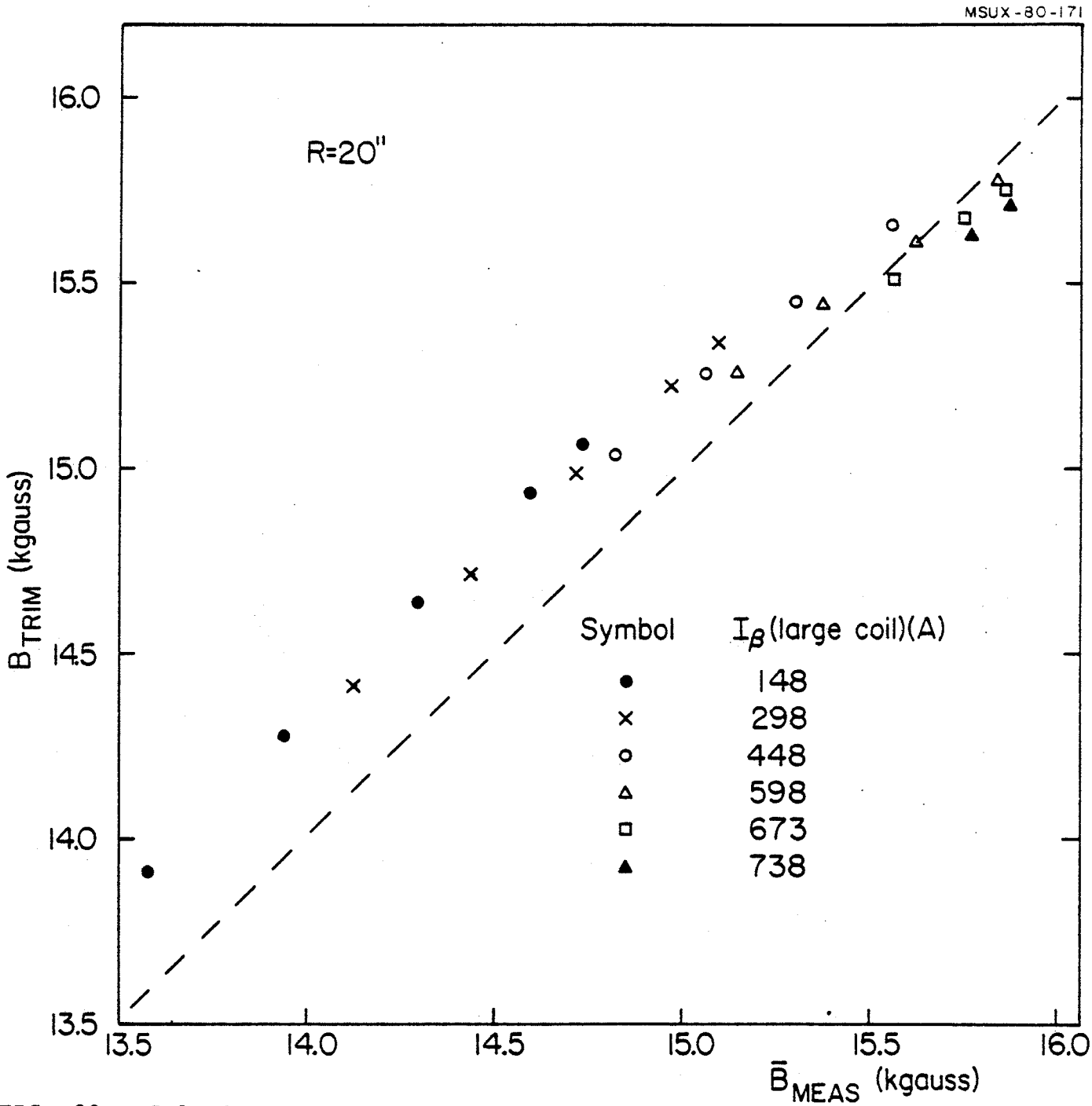

FIG. 29. Calculated versus measured average iron field at a radius of 20" for all the measured maps.

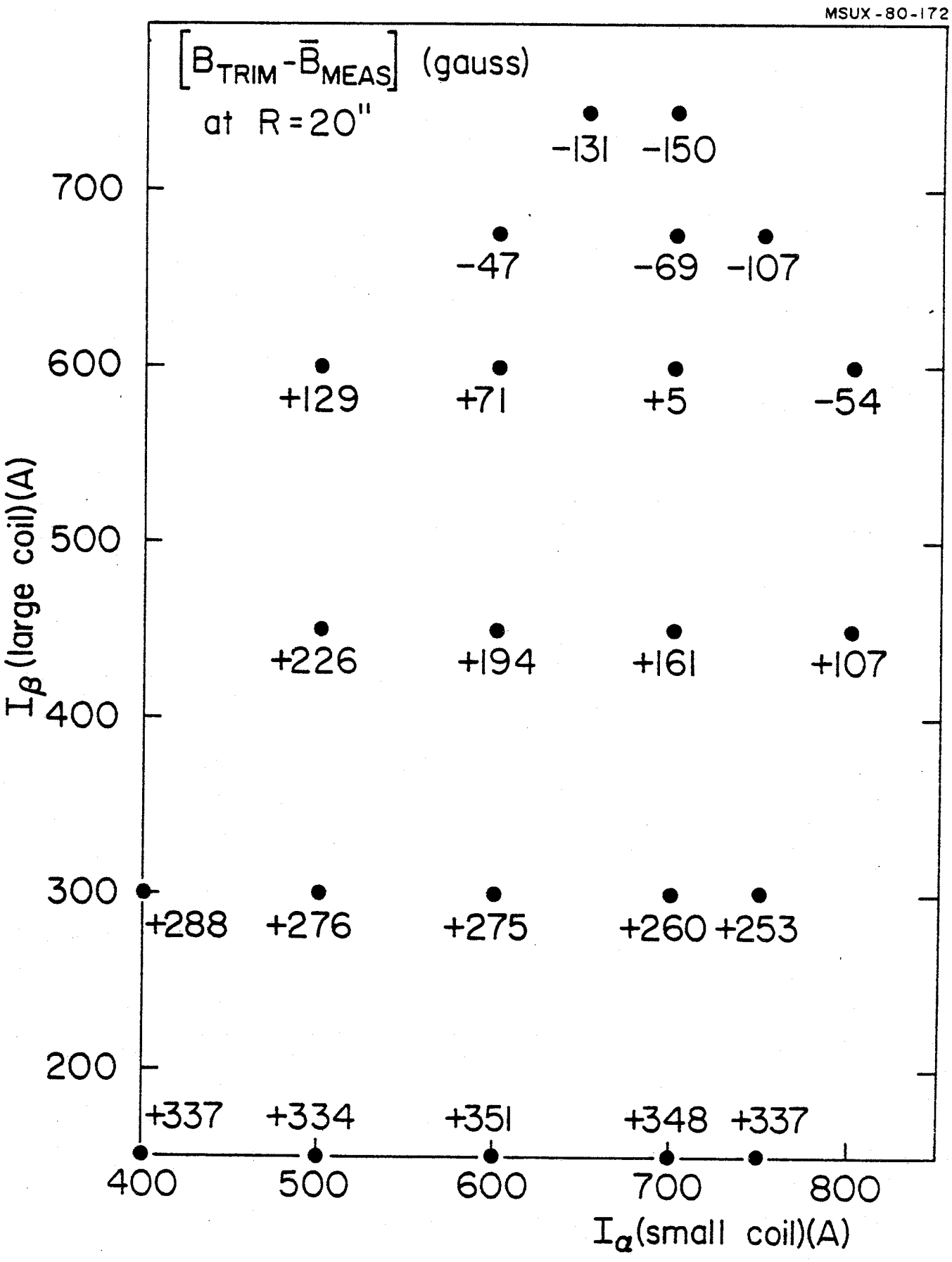

FIG. 30. Differences between calculated and measured average iron field in the plane (I_α, I_β) for all the measured maps.

usual (I_α,I_β) plane. As clear from both figures, at the lowest excitation, i.e. I_α=400 A and I_β=148 A, our model overestimates the field by 350 gauss. At an intermediate excitation of I_α=600 A and I_β=448 A, this reduces to 200 gauss, until at the highest excitation of I_α=700 A and I_β=738 A, the model underestimates the field by 150 gauss. If we recall that the observed total variation in the $\bar{B}_{iron}$ field is of the order of 2.8 kgauss, it is clear that our model gives essentially a variation range smaller by about 500 gauss, i.e. 20% less than measured.

As for the average field slope in the radial range from 5" to 25" a glance at Fig. 19 shows that the $\bar{B}_{iron}$ field decreases almost linearly between 10" and 20". The field slope between these two radii is therefore a good parameter to compare the calculated and measured fields. This is done in Fig. 31, where the calculated slope is plotted vs the measured one, for all 23 maps. The dashed line would correspond to perfect agreement. The general trend emerging from Fig. 31 is that the model underestimates the slope at low excitations i.e. tends to give a radially less decreasing field than measured. At high excitations the slope is instead overestimated, giving a faster decreasing field. However the error is rather confined, being at most of +3% for the highest excitations and -1.5% at the lowest ones. Our model seems therefore to reproduce the average slopes much better than the absolute values of the field the former being, as far as a cyclotron design is concerned, much more important than the latter.

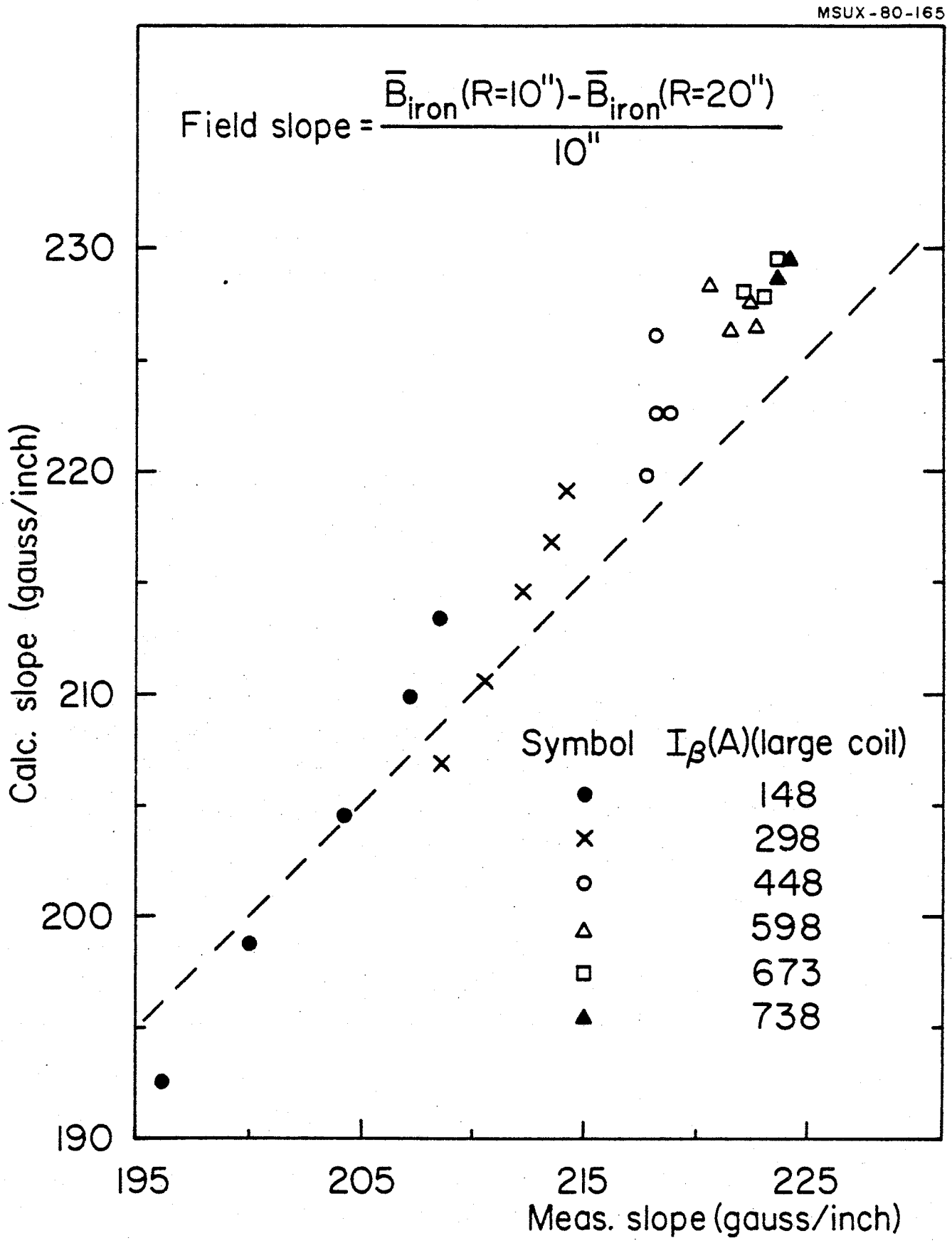

FIG. 31. Calculated versus measured iron field slope for all the measured maps.

The analysis of the discrepancies in the fringing field region (Figs. 27 and 28) is more involved. We have not been able to completely explain the observed pattern, since several effects must be taken into account when dealing with the fringing field region. Let us first recall that, as can be seen from Fig. 7, the radial range between 30" and 35" is the one where the coil-produced field changes sign and therefore the gradient is generally maximum. Consequently small errors in the main coil form factors can produce large differences in the field. The most likely causes of errors are the following:

- Coil contraction at liquid helium temperatures, even though confined to .3%. The difference in the air core fields between room temperature coils and cold coils is plotted in Fig. 32 for two different excitations. In order to extract the $\bar{B}_{iron}$ fields from the measured total fields, cold coil form factors have obviously been used in this work. However the size of the difference shown in Fig. 32 points out that small errors in the evaluation of the contraction can lead to non negligible errors in the fringing field estimate.
- Uncertainties in the coils dimensions. As an example Fig. 33 shows (curve 1) the effect of a variation of 50 mils in the coils distance from the median plane. Curve (3) of the same figure shows the effect of a variation of 50 mils in the coil radii. Both effects are rather large and point out that very accurate dimensions of the coils are needed to precisely calculate the field at 25" to 40".

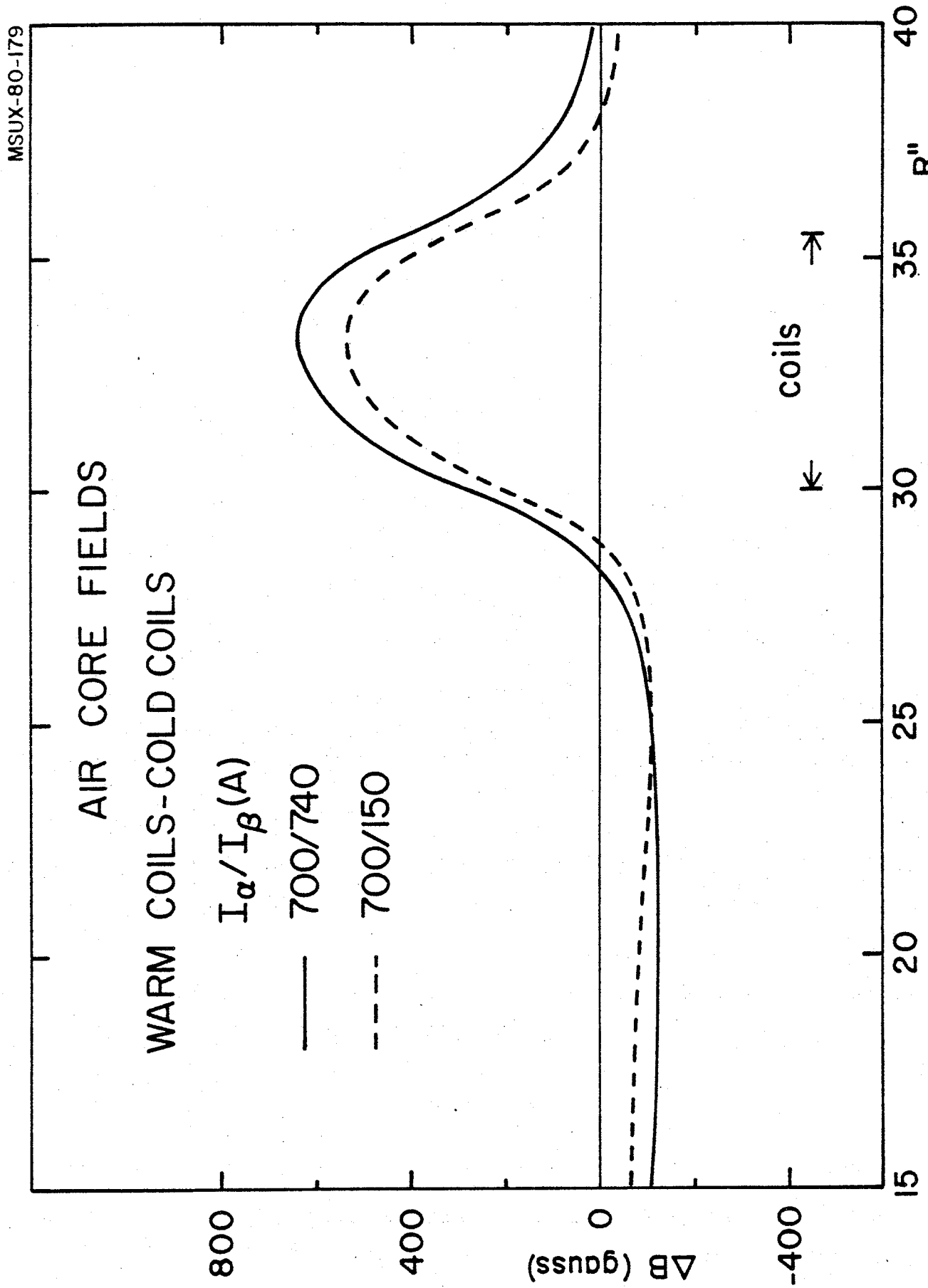

FIG. 32. Air core field differences between room temperature coils and cold coils for two excitations. The contraction factor is .3%.

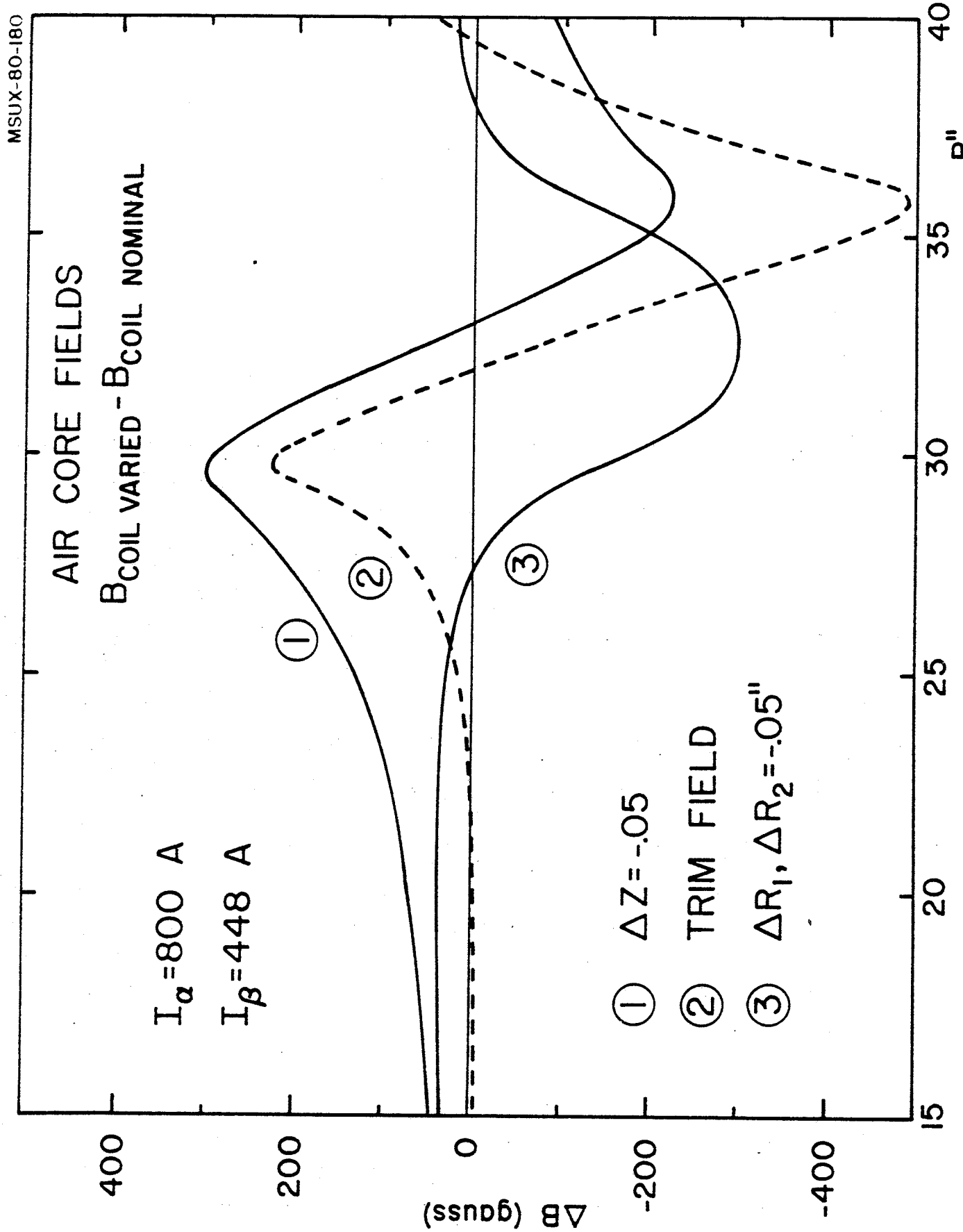

FIG. 33. Air core field differences, as a function of the radius, between a varied coil and a nominal coil. See text for details.

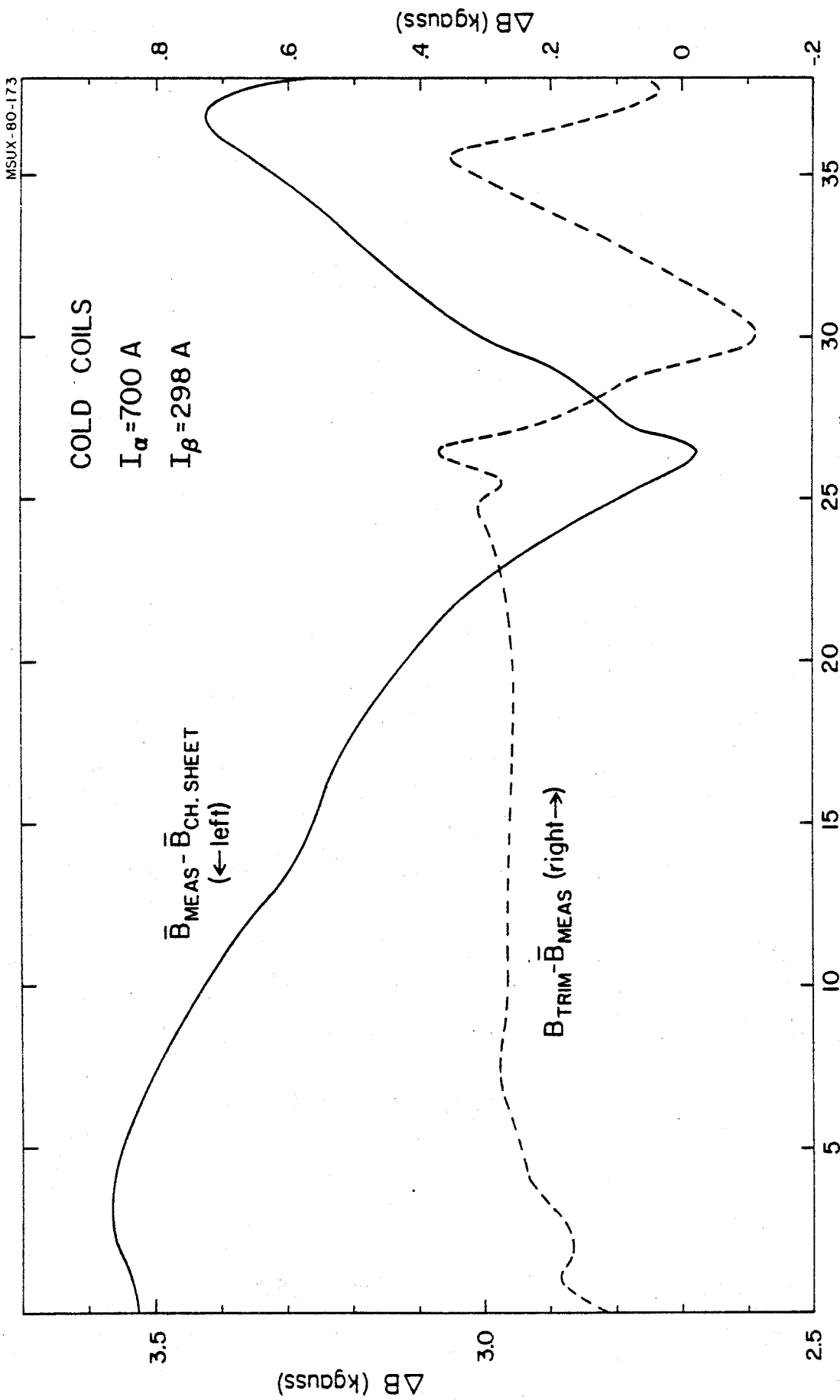

FIG. 34. Differences between calculated and measured average iron field as a function of the radius. B_{TRIM} represents the field calculated with the model described in the text, $B_{CH.SHEET}$ the field calculated with the uniform saturation of the pole tip.

- The mesh size in the grid used by TRIM for a magnet of this dimension makes it difficult, for the code, to precisely calculate the coil-produced field in this region. As an example, curve (2) of Fig. 33 shows the difference between an exact calculation of the coils field and the field given by TRIM when only the coils are taken into account, i.e. all iron has been suppressed from the TRIM grid.

The pattern of the errors produced by the causes just discussed are somewhat similar to the observed discrepancies. However we have been unable to single out one of these as the leading cause.

As a conclusion of this analysis we also would like to point out that if only the uniform saturation approximation is used to calculate the field, sizable errors both in the average field level and the slope would occur. This is shown in Fig. 34 in a self explanatory way.

6. Field Imperfections

The five 360^{o} maps yielded a detailed picture of the imperfections present in the field. Plots of the 1^{st} and 2^{nd} harmonics measured at all different excitations are shown in Figs. 35 and 36 respectively, both for the amplitude and phase.

The 1^{st} harmonic shows an iron-produced component, practically constant at all excitations, which peaks with an amplitude 8 gauss at 14", where the pole tips splitting

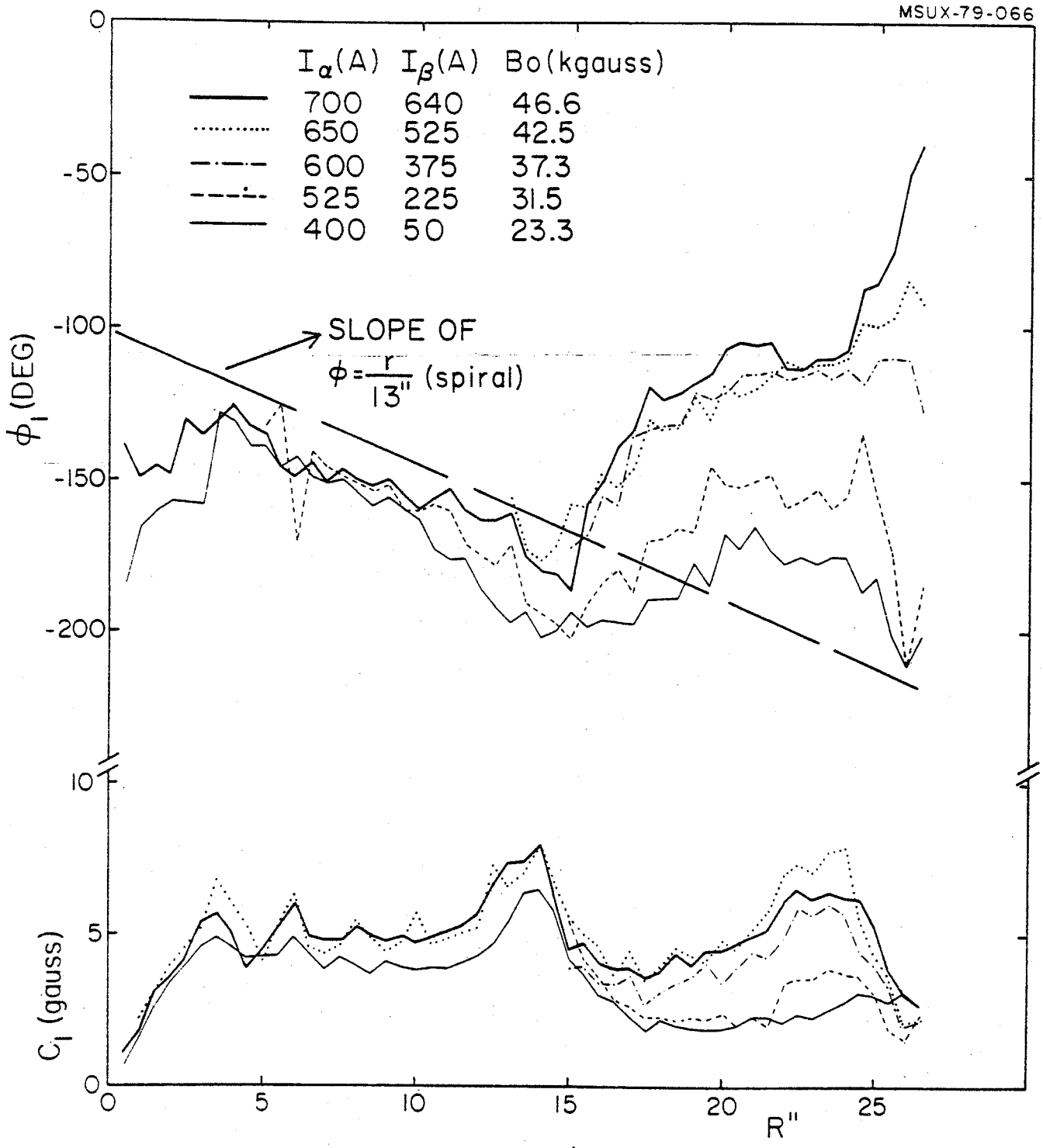

FIG. 35. Amplitude and phase of the 1st harmonic, as a function of the radius, measured at the listed coil currents.

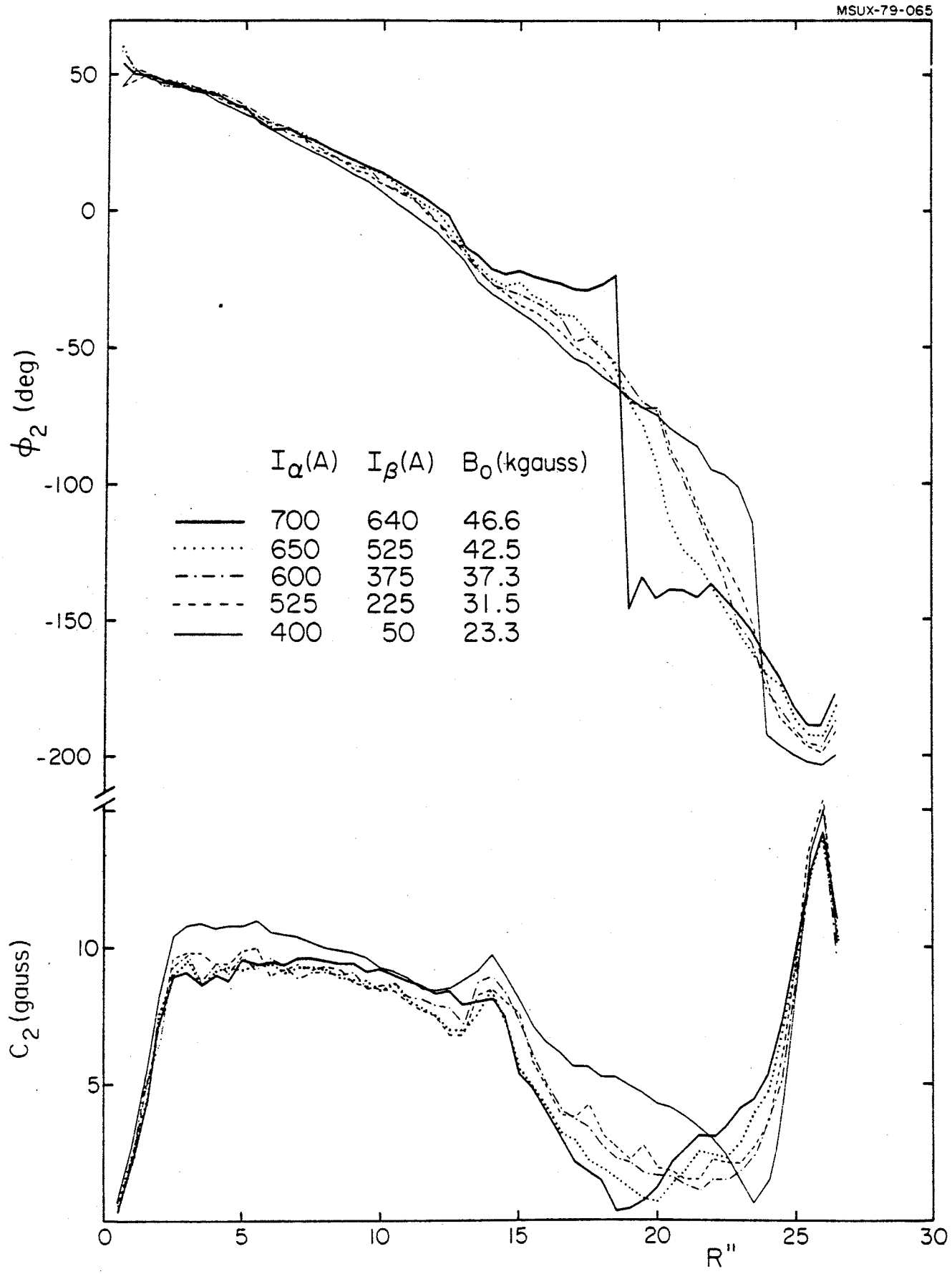

Fig. 36. Amplitude and phase of the 2nd harmonic, as a function of the radius, measured at the listed coil currents.

occurs, and has a phase very much coincident with the hill spiral. At outer radii, the dominant component comes from the coil-produced field. An off-centering error of the coils generates in fact a 1st harmonic which peaks at the radius where the radial gradient of the coil air-core field is maximum. Actually, the coils have been centered by minimizing the 1^{st} harmonic amplitude at a radius of 26",[9] which coincides roughly with the ν_R=1 radius. This result is indeed achieved, but as a consequence the first harmonic from the coils reaches an amplitude up to 6-7 gauss at 23"-24" radius. This should not have, however, any serious consequences on the beam.

The main feature of the 2^{nd} harmonic, Fig. 36, is a peak amplitude of 15 gauss at 26" radius, constant at all excitations. This has been traced back to an eccentricity of the tank inner wall. We may also note that a small peak in amplitude shows up again at the radius of the pole tips splitting, i.e. 14".

Measurements off the median plane were also carried out. The measuring bar was displaced by .31" axially, above and below the medium plane and maps taken over 360^{o}. The difference between the two can in principle reveal large errors in the median plane position. None of significance were found. Since the field off the medium plane can also be calculated to 3^{rd} order with the formula:

$$B_z(r,\theta,z) = B_z(r,\theta,0) - \frac{z^2}{2} L\, B_z(r,\theta,0)$$

whre L is the two dimensional Laplace operator, the data thus taken were compared to the predictions. The result is shown in Fig. 37, over a 120^{o} azimuthal interval. On the basis

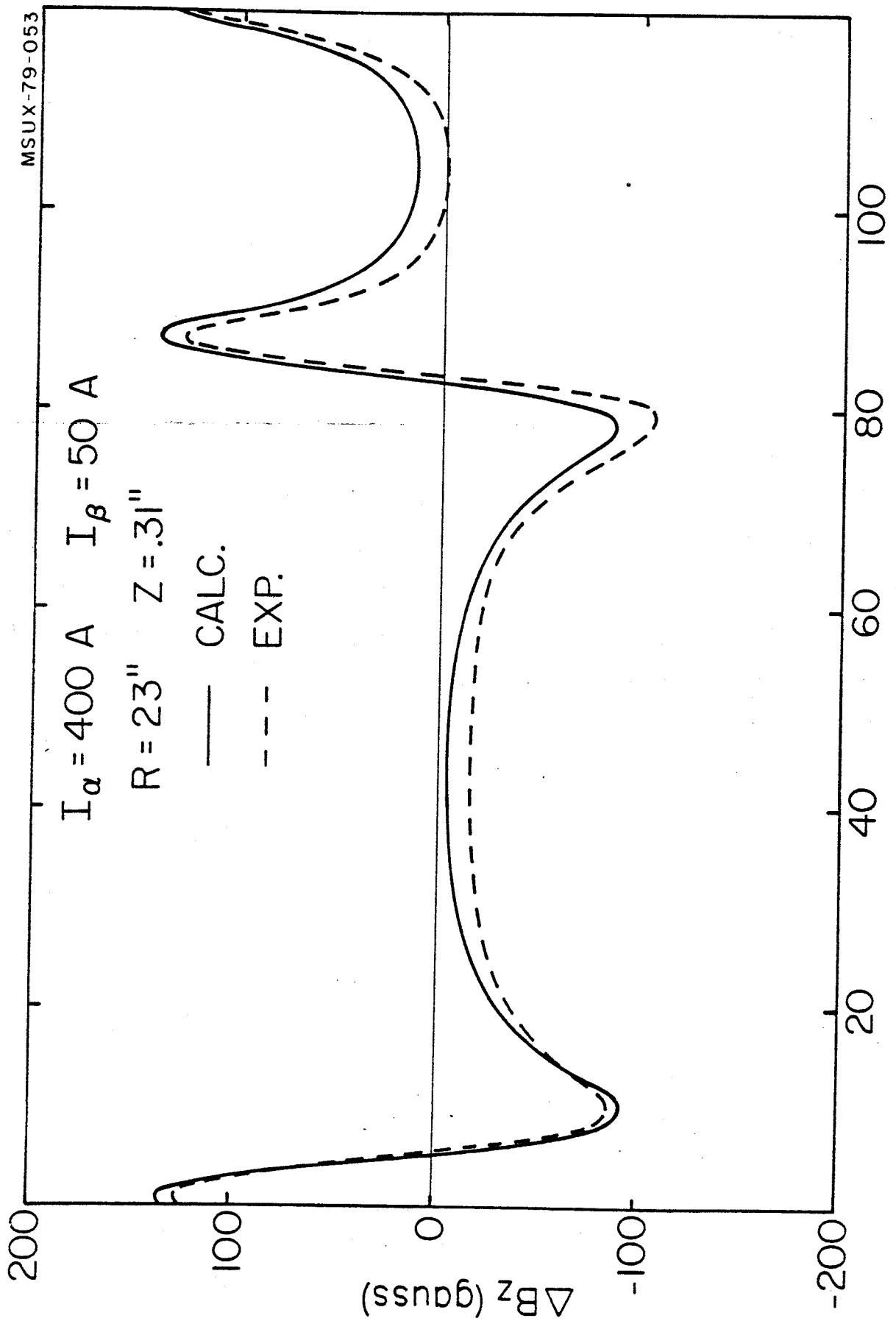

FIG. 37. Calculated and measured variation of the magnetic field, as a function of the azimuth at R=23", for a displacement of .31" from the median plane.

of these measurements it was concluded that median plane errors if present, are confined to less than $\pm$ 10 mils.

7. Conclusions

The analysis of the present data would support the conclusion that, as a whole, the computational methods used are quite adequate to properly design a superconducting cyclotron. No modeling is therefore necessary. However, the designer should be aware that:

- harmonics amplitudes may turn out to be off by 2%-3%, and have a rather complex pattern of variation with the coils excitation in the 1%-1.5% range. While this can be considered trivial in the design stage, it is not so for those beams at the limit of axial focusing. Some margin should therefore be anticipated.
- If our model for predicting the average fields is used, the absolute values of the iron-produced field can be off by 200-300 gauss in both directions, depending upon the coil excitations. However, since the code overestimates the field at low excitations (and viceversa), this does not require, in principle, a proportional margin on the number of ampereturns required in the coils.
- The predictions on the average field slope, although remarkably accurate, do in principle pose a more serious problem. In fact, although the discrepancy is confined to a few gauss/inch, this sums up to several tens of gauss over the typical 10-25" radial range. This can in turn affect predictions on the trim coil power required

for isochronizing the field at all excitations. However, since the difference is smoothed out over this same radial interval we find that different relative settings of the two coil sections do take care of it[2]. The situation could of course be entirely different for a model which, say, fails to reproduce the slopes that accurately.

- Large errors still may remain in the outer fringing field region. However, they are not going to influence the performance, say, of an extraction system, in such a way as to require major design changes. This stems from the fact that the radial position of the observed discrepancies is in the coil region. At this point any extracted beam is well on its way out, and therefore only minor changes in the parameters of the deflection system will be needed to adjust to a measured field configuration.

We do not foresee in the short-range dramatic changes in the picture presented here because, to the best of our knowledge, real three dimensional calculations are still a long way off. Therefore a precise and detailed mapping of the field will still be necessary in the foreseeable future. The design stage can however be pursued in good confidence, provided a "realistic" model for the average fields, like the one presented here, is available.

REFERENCES

1. H.G. Blosser, The Michigan State University Superconducting Cyclotron Program, IEEE Trans. Nucl. Sci. NS-26 (1979) 2040.
2. G. Bellomo and F. Resmini, Trimming of the Magnetic Field for the K-500 Cyclotron at MSU, to be published.
3. P. Miller et al., Magnetic Field Measurements in the MSU 500 MeV Superconducting Cyclotron, IEEE Trans. Nucl. Sci. NS-26 (1979) 2111.
4. H.G. Blosser and D.A. Johnson, Focusing Properties of Superconducting Cyclotron Magnets, Nucl. Instr. and Meth. 121 (1974) 301.
5. H.G. Blosser, et al., Superconducting Cyclotron General Description, MSU Annual Report 1974-1976, 95.
6. J.H. Ormrod et al., The Chalk River Superconducting Cyclotron, IEEE Trans. Nucl. Sci. NS-26 (1979) 2034.
7. E. Acerbi et al., Field Measurements on the Milan Superconducting Model Magnet, IEEE Trans. Nucl. Sci. NS-26 (1979) 2114.
8. J.S. Colonias, TRIM: A Magnetostatic Computer Program for the CDC 6600, UCRL-18439 (1968).
9. P. Miller et al., Centering of the Coil and the Cryostat in the K500 magnet, MSU Annual Report 1978-1979, 117.